Optimization of Design Factors of Hemodiafilter for Continuous Renal Replacement Therapy (CRRT) in terms of Solute Removal Performance

MU, Changjun / 牟, 倡駿

(開始ページ / Start Page)
1
(終了ページ / End Page)
104
(発行年 / Year)
2024-03-24
(学位授与番号 / Degree Number)
32675甲第601号
(学位授与年月日 / Date of Granted)
2024-03-24
(学位名 / Degree Name)
博士(理工学)
(学位授与機関 / Degree Grantor)
法政大学 (Hosei University)
(URL)
https://doi.org/10.15002/00030496

法政大学審査学位論文

Optimization of Design Factors of Hemodiafilter for Continuous Renal Replacement Therapy (CRRT) in terms of Solute Removal Performance

牟倡駿/Changjun Mu

Contents

Chapter 1

Development and Clinical Importance of Continuous Renal Replacement Therapy (CRRT)

Chapter 1 Development and Clinical Importance of Continuous Renal Replacement Therapy (CRRT)

1 Overview and Development of CRRT

Continuous renal replacement therapy (CRRT) is a blood purification treatment that continuously removes overloaded bodily fluids and excessive uremic toxins from the body through slow and steady extracorporeal blood circulation.[1] Compared with intermittent renal replacement therapy (IRRT), which usually lasts for 3-4 hours, several times a week, CRRT extends the treatment duration to 24 hours or a few days, fully simulating the continuity of renal function. An adequate treatment duration can reduce the requirement for solute removal efficiency per unit time, gently remove overloaded bodily fluids and excessive uremic toxins, minimize the impacts of changes in blood volume and solute concentration on the body, stabilize hemodynamics, and provide the homeostatic balance necessary in the treatment of critically ill patients. Furthermore, the adoption of high-flux and biocompatible membrane built-in blood purification devices (filters, hereafter) can improve the removal efficiencies of middle and high molecular weight solutes, reduce inflammation in critically ill patients, and efficiently regulate immune function. This chapter systematically describes the evolution of CRRT and the most advanced applications that could improve treatment efficiency.

1.1 The Inception of CRRT

In 1960, Scribner *et al.* established the concept of continuous blood purification, which was a treatment approach that continuously and slowly removed water and solutes for 24 hours.[2-3] However, specific clinical applications were not established because the basic principle of extracorporeal blood circulation was not sufficiently understood at that time; there were also

technical restrictions involving filters and devices. In 1967, Henderson *et al.* investigated the mechanism of convective mass transfer in blood purification; the rate of solute removal would be proportional to the applied pressure gradient and this could be adjusted to meet the needs of the clinical situation.[4-5] In 1977, based on the previous pioneering theoretical studies, Kramer *et al.* proposed continuous arterio-venous hemofiltration (CAVH) for patients with acute renal failure who cannot be treated with IRRT.[6] In this method, the patient's femoral artery supplied blood to the filter, and the purified blood was returned to the patient through the femoral vein. The difference in arterial and venous pressure was used as the driving force for extracorporeal blood circulation; a significant transmembrane pressure (*TMP*) was created between either side of the membrane, resulting in ultrafiltration. Because it was simple to operate, did not involve a blood pump and circulation control system, and did not require skilled medical experts, CAVH was frequently utilized in the intensive care unit (ICU); it was particularly useful for the treatment of patients with water retention who did not respond to diuretics. The clinical application of CAVH marked the emergence of a new blood purification technique, signaling the beginning of extracorporeal treatment in the ICU and leading to rapid development in subsequent decades.

In 1983, Lauer *et al.* conducted a rigorous analysis of the technical characteristics and therapeutic mechanisms of CAVH, further expanding the overall understanding of the concept of CRRT.[7] Compared with IRRT, CAVH had advantages such as hemodynamic stability, as well as slow and continuous solute removal; however, its ultrafiltration and solute removal capabilities were limited. The ultrafiltration flow rate (Q_{UF}) of CAVH was 12–18 L/24 hr, the maximum daily clearance of urea did not exceed 18 L/24 hr.[8] Thus, in a patient with a mean urea concentration of 1 g/L, urea removal in 24 hours could not exceed 18 g. Low solute removal efficiency might result in insufficient management of urea in patients with severe metabolic diseases, leading to treatment failure. In 1984, Geronemus *et al.* reported the first use of a cellulose membrane dialyzer for continuous arterio-venous hemodialysis (CAVHD).[9] They used a blood flow rate (Q_B) of 100 mL/min and a dialysate flow rate (Q_D) of 1 L/hr (= 16.7 mL/min). Because Q_D was significantly lower than Q_B, the urea clearance (C_L) was nearly equal to Q_D; with a modest amount of ultrafiltration, the daily clearance could be increased to 24–26 L/24 hr, which significantly improved the removal efficiencies of low molecular weight solutes. In 1985, Ronco *et al.*

proposed continuous arterio-venous hemodiafiltration (CAVHDF) and applied it to multiple organ dysfunction syndrome (MODS).[10] Using a combination of diffusion and convection, CAVHDF slightly increased the removal efficiencies for low molecular weight solutes, while significantly improving the removal efficiencies of middle and high molecular weight solutes. CRRT has gradually gained worldwide recognition and has entered a stage of rapid development.

1.2 Technological Innovations in Vascular Pathways

To overcome the limitations of CAVH (e.g., risks of bleeding, thrombosis, and infection, as well as the inability to treat patients with severe hypotension), Bischoff *et al.* proposed continuous veno-venous hemofiltration (CVVH) in 1979 to treat patients with acute renal failure after cardiac surgery.[11] CVVH utilized a dual vena cava catheter to establish a blood circulation pathway, a blood pump to drive blood circulation, and a balance control system to monitor volume. Even in poor cardiovascular conditions, CVVH was able to achieve considerable ultrafiltration and efficient solute removal. The development of a vascular pathway from arterio-venous mode to veno-venous mode significantly reduced the risk of vascular pathway-related complications and improved treatment safety. With the development of dual vena cava catheters, blood pumps, and ultrafiltration balance control systems in the late 1980s, CVVH rapidly replaced CAVH and became the standard mode of treatment in the ICU.[12-14] In 1988, Tam *et al.* proposed continuous veno-venous hemodialysis (CVVHD).[15] In 1993, Ronco reported clinical application of continuous veno-venous hemodiafiltration (CVVHDF).[16] New treatment modes such as CVVH, CVVHD, and CVVHDF have been derived from the initial CAVH involving the arterio-venous pathway; all have been successfully used in clinical settings. CRRT has created a new system for acute renal replacement therapy.

1.3 Expansion of the CRRT Concept

Nephrology and intensive care are independent specialties; the development of CAVH led to the creation of a new medical specialty, critical care nephrology, along with parallel development

of blood purification technology in critical care medicine.[17] In 1985, Wendon *et al.* proposed continuous high-volume veno-venous hemofiltration (continuous HVHF) to improve hemodynamics by increasing ultrafiltration volume.[18] In 1993, Ronco *et al.* proposed continuous high-flux dialysis (CHFD), which increased convection to compensate for insufficient removal efficiencies of middle molecular weight solutes, resulting in urea daily clearance of 60 L/24 hr (= 41.7 mL/min) and inulin daily clearance of 36 L/24 hr (= 25.0 mL/min).[19] In 1998, Tetta *et al.* introduced continuous plasma filtration adsorption (CPFA) for the removal of inflammatory mediators and endotoxins.[20] In addition to advancements in treatment modes, there has been continuous evolution of high-flux and biocompatibility membranes for CRRT,[21] as well as blood purification devices with precise volume balance control systems.[22-23] The combined evolution of these three factors (membranes, blood purification devices, and volume balance control systems) has contributed to the maturation and advancement of the CRRT medical concept and related technologies.

Prior to the 1990s, there was no standardized naming convention for CRRT. The first International CRRT Academic Conference was held in 1995; the relevant terminology of CRRT was standardized during that conference.[24] The primary naming foundation for each treatment mode is based on operational technique characteristics, with an emphasis on water and solute removal mechanisms; it excludes specific filters, pipelines, and other components.[25] Since the year 2000, clinical applications of CRRT have expanded beyond basic kidney replacement to include sectors other than kidney disease. During the 9th International CRRT Academic Conference in 2004, Ronco *et al.* extended CRRT to multiple organ support therapy (MOST).[26] CRRT is now commonly utilized in the treatment of acute kidney injury (AKI), MODS, systemic inflammatory response syndrome (SIRS), sepsis, acute respiratory distress syndrome (ARDS), severe heart failure, liver failure, metabolic acidosis, severe electrolyte abnormalities, toxin (drug) poisoning, and other diseases. It has evolved into an essential support measure that facilitates the recovery of various critically ill patients.

2 Main Treatment Modes of CRRT

Through more than 40 years of clinical practice and technological innovation, CRRT has developed from its initial basic concepts to encompass four core treatment modes and numerous derivative treatment modes.

2.1 Four Core Treatment Modes

The four core treatment modes are categorized according to complexity as slow continuous ultrafiltration (SCUF), CVVH, CVVHD, and CVVHDF (Table 1).[27]

Table 1. Comparison of treatment modes.

Treatment mode	SCUF	CVVH	CVVHD	CVVHDF
Q_B [mL/min]	50–100	100–250	100–200	100–200
Q_D [mL/min]	–	–	16.7–33.4	16.7–33.4
Q_{UF} [L/hr]	0.1-0.2	1–4	–	1–2
Q_R [L/hr]	–	0.9–3.8	–	1–1.8
Membrane permeability	High	High	High	High
Clearance for LMs	–	+++	+++	+++
Clearance for MMs	–	+++	+	+++
Solute removal mechanism	Convection	Convection	Diffusion	Both

SCUF, slow continuous ultrafiltration; CVVH, continuous veno-venous hemofiltration; CVVHD, continuous veno-venous hemodialysis; CVVHDF, continuous veno-venous hemodiafiltration; Q_B, blood flow rate; Q_D, dialysate flow rate; Q_{UF}, ultrafiltration flow rate; Q_R, replacement solution flow rate; LMs, low molecular weight uremic toxins; MMs, middle molecular weight uremic toxins; +, simplest; +++, most difficult.

(1) Slow Continuous Ultrafiltration (SCUF)

SCUF mainly removes excess water through ultrafiltration (Figure 1).[24] The Q_B is usually set at 50–100 mL/min, and no dialysate or replacement solution is required. A modest amount of ultrafiltration is conducted with a Q_{UF} of 0.1–0.2 L/hr. SCUF has a low solute removal capacity and is primarily used to correct bodily fluids overload. It is ineffective as treatment for solute imbalance-related internal environmental disorders.

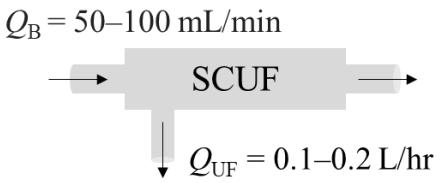

Figure 1. Principle of slow continuous ultrafiltration (SCUF).[24]

Q_B, blood flow rate; Q_{UF}, ultrafiltration flow rate.

(2) Continuous Veno-venous Hemofiltration (CVVH)

CVVH uses a dehydration pump to apply negative pressure from the outside of the hollow fiber membrane, removing overloaded bodily fluids through ultrafiltration; this results in convective removal of low and middle molecular weight solutes. Simultaneously, electrolyte balance is maintained by supplementing the replacement solution without requiring dialysate (Figure 2).[24] The Q_B is often set at 100–250 mL/min, Q_{UF} is set at 1–4 L/hr, and the replacement solution flow rate (Q_R) is set at 0.9–3.8 L/hr. There are two types of fluid replacement (alternately called "dilution" or "substitution") methods: pre-dilution and post-dilution. Pre-dilution is equivalent to diluting the blood flowing into the filter, which can inhibit concentration polarization and membrane fouling, decrease heparin dosage, and reduce the rate at which coagulation events occur in the filter. However, pre-dilution has a lower solute removal efficiency, compared with post-dilution, because it simultaneously dilutes the concentration of solutes in the blood, leading to a reduced concentration gradient.

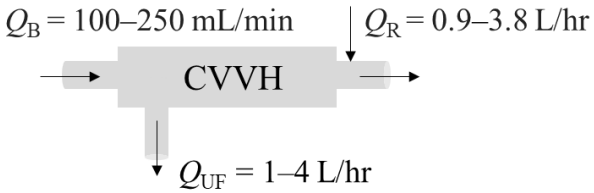

Figure 2. Principle of post-dilution continuous veno-venous hemofiltration (post-dilution CVVH).[24] Q_B, blood flow rate; Q_{UF}, ultrafiltration flow rate; Q_R, replacement solution flow rate.

(3) Continuous Veno-venous Hemodialysis (CVVHD)

CVVHD uses a blood pump to drive blood circulation, and dialysate flows outside of the hollow fiber membrane counter currently or in the opposite direction relative to blood flow (Figure 3).[24] The concentration gradient on either side of the hollow fiber membrane is the driving force, and solutes are mainly removed by diffusion. The Q_B is often set at 100–200 mL/min, and Q_D is set at 16.7–33.4 mL/min. Because the Q_D is substantially lower than the Q_B, the C_L is nearly equal to Q_D; this facilitates a complete blood-dialysate concentration balance. Compared with CVVH, CVVHD causes less stress on the membrane, is less likely to cause pore blockage, and does not require replacement solution. CVVHD has excellent removal performance for low molecular weight solutes but is inferior to CVVH in the removal performance of middle molecular weight solutes. CVVHD is more appropriate for AKI patients with severe catabolic problems.

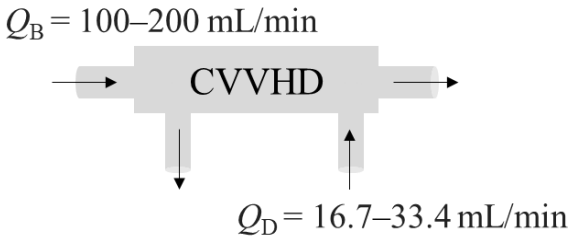

Figure 3. Principle of continuous veno-venous hemodialysis (CVVHD).[24]

Q_B, blood flow rate; Q_D, dialysate flow rate.

(4) Continuous Veno-venous Hemodiafiltration (CVVHDF)

CVVHDF combines the diffusion features of CVVHD with the convective properties of CVVH, thereby improving the removal efficiencies of low molecular weight solutes while effectively removing middle molecular weight solutes with molecular weight of 30–40 kDa (Figure 4).[28] The Q_{UF} is typically restricted to 2 L/hr. Compared with CVVHD and CVVH, CVVHDF allows more accurate management of bodily fluids, electrolytes, and acid-base balance; improves tissue oxygen metabolism; improves respiratory function by minimizing pulmonary interstitial edema; and provides adequate nutritional support. CVVHDF is the most effective treatment approach for MODS.[29]

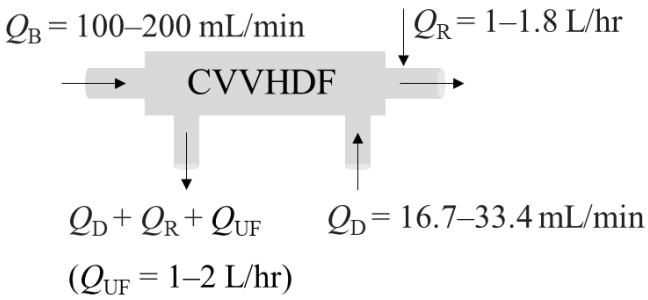

Figure 4. Principle of post-dilution continuous veno-venous hemodiafiltration (post-dilution CVVHDF).[24] Q_B, blood flow rate; Q_D, dialysate flow rate; Q_{UF}, ultrafiltration flow rate; Q_R, replacement solution flow rate.

2.2 Important Derivative Treatment Modes

Critically ill patients frequently have severe metabolic imbalances, which cause a sustained increase in the levels of systemic inflammatory mediators. Important treatment modes such as continuous HVHF, CHFD, and CPFA have been derived to improve the removal efficiencies of inflammatory mediators. In clinical practice, the most appropriate CRRT mode is selected based on the severity of the patient's condition, as well as the underlying causes.

(1) Continuous High-Volume Veno-venous Hemofiltration (Continuous HVHF)

Continuous HVHF is a CVVH derivative mode that can be implemented in two ways: either maintain Q_{UF} at 3–4 L/hr and receive standard CVVH, or maintain standard CVVH overnight but use a Q_{UF} of 6–8.4 L/hr during the day to achieve a total ultrafiltration volume of 60–100 L/24 hr.[30] A substantial amount of ultrafiltration in continuous HVHF requires the use of high-volume filters with membrane areas of 1.6–2.2 m^2. Compared with standard CVVH, continuous HVHF allows more effective removal of inflammatory mediators; it is appropriate for the management of sepsis and septic shock.[31]

(2) Continuous High-Flux Dialysis (CHFD)

CVVHD has high removal efficiencies for low molecular weight solutes but low removal efficiencies for middle molecular weight solutes. CVVHDF requires a considerable amount of replacement solution. CHFD was created as a derivative mode of CVVHD that combines the benefits of CVVHD and CVVHDF, ensures appropriate convection and diffusion intensities, and reduces the amount of replacement solution.[30] CHFD consists of a CVVHD system and a dialysate volume control system.[32] Two pumps are used to manage the ultrafiltration process. The first pump transports the heated dialysate into the filter; the second pump regulates the outlet flow of the dialysate, thereby controlling ultrafiltration. Compared with CVVHD and CVVHDF, CHFD provides more effective control of ultrafiltration and convection without using replacement solution, thereby improving the removal efficiencies of middle and high molecular weight solutes.

(3) Continuous Plasma Filtration Adsorption (CPFA)

CPFA is a combination treatment mode that comprises adsorption and standard CRRT. Whole blood is separated by a plasma separator; the separated plasma is perfused into an immune adsorbent, then recombined with blood cells and pumped into a high-flux filter.[33] The Q_B is often set at 50–200 mL/min, and no replacement solution is required. Compared with CVVHD, CPFA

can improve hemodynamics in critically ill patients by maintaining balance among bodily fluids, electrolytes, and acid-base interactions, while efficiently removing inflammatory mediators, endotoxins, and activated complement; thus, it regulates the body's immune system and improves survival.[34]

3 Clinical Benefits of CRRT

The primary clinical benefits of CRRT include maintaining metabolic stability, reducing fluctuations in osmotic pressure, maintaining stable hemodynamics, providing continuous and stable bodily fluids management, facilitating nutritional support, and removing inflammatory mediators, all of which improve the prognosis of critically ill patients.

3.1 Maintenance of Balance Among Bodily Fluids, Electrolytes, and Acid-Base Interactions

The Q_B of IRRT is often set at 200–250 mL/min, whereas the Q_D is set at 500–800 mL/min. Although IRRT can remove large amounts of bodily fluids and solutes in a short period of time, rapid changes in water and solute concentrations often cause a sudden drop in blood pressure. In critically ill patients, severe disease often hinders independent volume regulation and causes poor tolerance to volume variations. Small imbalances in bodily fluids can aggravate electrolyte and acid-base abnormalities, resulting in acute pulmonary edema, brain edema, and other conditions. Furthermore, the intermittent nature of IRRT can lead to "non-physiological" increases in toxins such as urea and creatinine, generating significant oscillation in the internal environment.[35] In contrast, CRRT fully mimics the continuous filtration function of glomeruli; it avoids significant variations in electrolyte and acid-base balance by adjusting treatment parameters and the compositions of dialysate and replacement solution, thus maintaining better adherence to physiological conditions. A study comparing intermittent hemodialysis (IHD) and CVVHD showed that the mean urea level during IHD was 2.1 g/L, whereas the mean concentration during CVVHD significantly decreased and could be maintained at 1.4 g/L.[36] Additionally, when serum

sodium concentrations decline below 105 mmol/L, the mortality rate can reach 60% among patients with acute hyponatremia. Sodium imbalance correction requires an increase or decrease in bodily fluids volume. After 48 hours of CVVH, patients with clinically confirmed severe acute hyponatremia displayed a significant increase in serum sodium concentration from 100.9 mmol/L to 140.3 mmol/L.[37]

3.2 Hemodynamic Stability

Dialysis hypotension is one of the most common and serious complications in IRRT, affecting 20%–50% of patients; it can lead to cessation of therapy in up to 5% of patients.[21, 38] These outcomes arise because large amounts of water and solutes are removed in a short period of time, resulting in reductions of plasma refilling rate and venous volume, as well as a decrease in plasma osmotic pressure that exceeds standard compensatory mechanisms.[39] Some patients are susceptible to decreased sympathetic nerve tone, which leads to a decrease in arteriolar resistance, an increase in the transmission of pressure to veins, and a corresponding increase in venous volume. When blood volume is low, an increase in venous blood volume reduces cardiac filling and cardiac output, eventually causing hypotension. Repeated episodes of transient hypotension during dialysis can cause renal ischemic damage, thereby increasing the risks of heart disease and other complications associated with poor prognosis. Based on clinical symptoms, CRRT can promptly adjust bodily fluids balance, stabilize the renin–angiotensin system, improve the body's response to vasoactive substances, maintain proper organ perfusion, and stabilize extracellular fluid osmotic pressure; thus, it maintains hemodynamics, reduces the incidence of dialysis hypotension, and protects residual renal function, along with the functions of other organs.[40-41] Manns *et al.* observed that 27 AKI patients undergoing IHD displayed a 50% decrease in urine output after treatment, whereas 16 CVVHD patients displayed a 10% decrease.[42] Another study showed that arterial pressure decreased by 6 mmHg during IHD, whereas it decreased by 2 mmHg during CVVHD.[43]

3.3 Regulation of Volume Load and Provision of Adequate Nutritional Support

When intravenous fluids, blood products, parenteral nutrition, or other supportive medications are administered to critically ill patients, the kidneys cannot reliably maintain bodily fluids balance; thus, volume overload occurs and the organ function may be impaired.[44] There is a complex interaction between volume overload severity and mortality risk. CRRT is unique in that it intervenes at three levels of humoral control.[45-46] The first level of control involves calculating the Q_{UF} through estimation of the requirement for bodily fluids removal within 24 hours. Although this is similar to IRRT, the treatment duration differs. For example, the removal of 3 L of water during 4-hour IHD requires a Q_{UF} of $\geq$ 12.5 mL/min. Rapid dehydration can readily cause dialysis hypotension and limit dehydration volume. To achieve equivalent removal efficacy via continuous 24-hour CRRT, the Q_{UF} must reach 2.1 mL/min. The second level of control involves exceeding the hourly ultrafiltration volume above the intake value and achieving net bodily fluids balance via supplementation with replacement solution. This continuous treatment provides nearly unlimited drainage options. At any time, the bodily fluids status can be adjusted to net positive, net negative, or balanced, which helps to remove tissue edema, improve oxygen metabolism, and achieve bodily fluids balance in the body. The third level of control involves maintaining a stable hemodynamic condition with parameters such as central venous pressure, pulmonary artery wedge pressure, and mean arterial pressure, while ensuring the required hourly net bodily fluids balance.

CRRT can achieve a high ultrafiltration volume with a Q_{UF} of > 50 L/24 hr; the ultrafiltration volume is equivalent to the overall bodily fluids volume of an average-sized adult. A high-capacity load control capability can ensure adequate nutritional support. Bellomo *et al.* compared 84 AKI patients undergoing IHD with 83 patients undergoing CRRT; they found that the prescribed nutrition was received by 90% of the CRRT patients and 54% of the IHD patients.[47] McDonald *et al.* observed that IHD patients ingested 77% of the prescribed protein mass each day, whereas CRRT patients consumed 12% more protein mass than prescribed.[48] To compensate for poor removal volume, parenteral nourishment is frequently limited during IRRT, increasing the risk of malnutrition. CRRT allows full nutrient input without concerns about volume overload, facilitating more comprehensive nutritional support.[49]

3.4 Removal of Waste Products and Re-establishment of Internal Homeostasis

Because of functional decline in organs such as the heart, lungs, and kidneys, the bodies of critically ill patients accumulate large amounts of waste products and toxins that cannot be effectively removed. Critically ill patients are susceptible to various internal environmental disorders. Because solutes of interest differ in terms of molecular weight, distribution volume, half-life, hydrophobicity, and other aspects, appropriate treatment approaches must be chosen based on solute characteristics. For example, the blood of critically ill patients contains high concentrations of water-soluble inflammatory mediators with anti-inflammatory and pro-inflammatory effects, such as tumor necrosis factor (TNF)-α, interleukin (IL)-1, IL-6, and platelet activating factor (PAF). Because inflammatory mediators exhibit synergistic, redundant, autocatalytic, and self-enhancing properties, blocking or removing a single mediator cannot effectively improve a patient's condition. CRRT can continuously and non-selectively remove inflammatory mediators by increasing convection (continuous HVHF) or via combination therapy (CPFA), thereby effectively controlling the body's immune system and rapidly re-establishing immune homeostasis.[44]

4 Main Clinical Applications of CRRT

CRRT has two primary clinical applications: the treatment of kidney diseases (e.g., AKI or other organ dysfunction), and the treatment of critically ill patients with non-renal damage (e.g., SIRS, sepsis, MODS, and toxin (drug) poisoning).

4.1 CRRT in the Treatment of Kidney Diseases

(1) Acute Kidney Injury (AKI)

AKI is defined as the loss of renal function in a short period of time. The clinical criteria are a serum creatinine level that increases by > 3 mg/L within 48 hours or by > 50% from the baseline

value, or a urine volume of < 0.5 mL/(kg ħr) persists for 6 hours; the duration of disease must not exceed 7 days.[51] AKI can cause abnormal plasma concentrations of potassium, calcium, phosphorus, and magnesium in serum, leading to various electrolyte homeostasis disorders. Moreover, it can impair a patient's capacity to metabolize fixed acids, induce metabolic acidosis, and affect acid-base homeostasis; it can also cause high-volume load, hypertension, and systemic inflammation, thereby affecting cardiac function and triggering a systemic oxidative stress response.

Global population aging has led to increases in AKI incidence and mortality; thus, AKI is a global public health problem.[52] AKI occurs in 5%–7% of hospitalized patients and 20%–50% of ICU patients.[53] A multicenter study involving 40 ICUs across 16 countries showed that approximately 70% of AKI patients undergo progression to MODS.[54] Furthermore, according to the Kidney Disease Improving Global Outcomes (KDIGO) meta-analysis published in 2013, the mortality rate among adult AKI patients was 23.9%; the mortality rate among such patients requiring kidney replacement therapy was 49.4%.[55] For AKI patients with severe internal homeostatic imbalances, CRRT can enhance solute removal efficiencies, prevent additional kidney damage, and promote the recovery of renal and cardiac functions while preserving hemodynamics and managing balance among bodily fluids, electrolytes, and acid-base interactions. Thus, CRRT is the preferred method for treatment of AKI.[56]

(2) AKI with Cerebral Edema

AKI with brain edema can be caused by brain trauma, severe surgery, or other factors. Because plasma osmotic pressure rapidly decreases, IRRT is likely to increase osmotic pressure in brain tissue, allowing water to enter the brain tissue and causing dialysis imbalance syndrome; therefore, IRRT cannot be utilized to treat AKI with cerebral edema. The increase in intracranial pressure is also related to a rapid decline in mean arterial pressure during therapy, which results in decreased cerebral perfusion pressure. This scenario can only be managed by utilizing high-sodium, low-temperature dialysate and minimizing blood volume changes, which are challenging objectives for IRRT. During CRRT, the initial sodium ion concentration of the replacement

solution can be set to > 140 mmol/L, and treatment can begin at a low dose of 1 L/hr.[57] Slow changes in blood urea nitrogen levels and low molecular weight solutes help to maintain a positive sodium balance in the body and decrease the impact on intracranial pressure; the replacement solution flow rate can be gradually increased when the patient's condition has stabilized.

4.2 CRRT in the Treatment of Non-renal Diseases

(1) Sepsis, Severe Sepsis, Septic Shock, and Multiple Organ Dysfunction Syndrome (MODS)

Critical illness caused by severe trauma, infection, hemorrhage, shock, and other causes typically progresses through six stages (severe injury, SIRS, sepsis, severe sepsis, septic shock, and MODS) prior to mortality. Endogenous immune inflammatory mediators are produced when the body is exposed to exogenous injury or infection, triggering the initial inflammatory response. In critically ill patients, SIRS can develop because of diminished compensatory anti-inflammatory mediator capacity and metabolic dysfunction. Excessive inflammatory response activation causes a loss of control regarding the reaction mechanism, leading to the cascade-like release of inflammatory mediators such as TNF-α, IL-1, and IL-6 that can directly impair immune function. Simultaneously, excessive inflammatory mediators entering multiple circulatory systems can cause damage to endothelial cells and parenchymal cells throughout the body. The pathological stage of sepsis develops when pathogenic microorganisms (e.g., bacteria) invade the body and cause serious endogenous infections. Severe sepsis is characterized by organ malfunction, inadequate tissue perfusion, or hypotension. Irreversible septic shock involves persistent hypotension and hypoperfusion that cannot be corrected by sufficient fluid resuscitation and vasoactive drug intervention; affected patients display worsening organ dysfunction and subsequent progression to MODS, a clinical syndrome characterized by the simultaneous or sequential of two or more organs or systems, a complex and dynamic inflammatory process that indicates the patient's condition has become extremely severe.[58]

Sepsis occurs in more than 50% of ICU patients; the corresponding mortality rate increases

with age, from 10% in infants to 38.4% in patients aged > 85 years.[59] Severe sepsis and septic shock have mortality rates of 50% and 68%, respectively.[60] Although the imbalance between anti-inflammatory and pro-inflammatory mediators in a patient's body is the underlying cause of clinical worsening, the excessive production of both anti-inflammatory and pro-inflammatory mediators is difficult to control; the complex immune responses generated by these mediators can limit the effectiveness of many treatment methods. CRRT can effectively remove inflammatory mediators, endotoxins, lymphatic factors, and other factors from blood; reduce the peak blood concentrations of anti-inflammatory and pro-inflammatory mediators; control the imbalance between inflammatory responses and immunosuppressive mechanisms; improve endothelial cell dysfunction; re-establish immune homeostasis; and improve cardiovascular function by interfering with the expression of myocardial inhibitory factors and endothelin.[61] Furthermore, CRRT can improve hemodynamics, restore arterial wall tension, correct vascular paralysis in sepsis, reduce pulmonary vascular resistance, and enhance hepatic perfusion, thereby minimizing the dosages of vasopressors (e.g., dopamine and norepinephrine) during the treatment process. Zhang *et al.* demonstrated that after 72 hours of CVVH, the plasma concentrations of IL-1, IL-2, and IL-10 in sepsis patients dramatically decreased.[62] Smaller decreases in the concentrations of IL-6 and TNF-α were also observed; patient prognoses significantly improved after the removal of excessive inflammatory mediators. Additionally, Cole *et al.* prospectively investigated the impacts of HVHF and CVVH on hemodynamics in patients with sepsis and MODS in a randomized controlled trial.[63] After treatment, mean arterial pressure, central venous pressure, and cardiac index remained within target ranges; patients undergoing HVHF showed significant decreases in the concentrations of TNF-α and IL-6, whereas patients undergoing CVVH showed significant decreases in the concentrations of complement factors (e.g., C3a and C5a).

(2) Acute Respiratory Distress Syndrome (ARDS)

ARDS is characterized by widespread destruction of pulmonary capillary endothelial cells and alveolar epithelial cells as a result of severe trauma, infection, or major surgery; these changes lead to fluid accumulation in the alveoli and pulmonary interstitial edema. Because the lungs are

unable to inhale an adequate amount of air, oxygen entry into the blood is diminished; patients experience increasing respiratory discomfort, persistent hypoxemia, and other symptoms. Prior to the clinical application of CRRT, ARDS-related mortality approached 100% in patients with AKI. CRRT alleviates local inflammatory reactions in the lungs by removing pathogenic inflammatory mediators and reducing pulmonary capillary permeability; in addition to allowing water in pulmonary interstitial tissue to re-enter the blood, these changes reduce interstitial edema and improve cardiopulmonary function.[64] CRRT also corrects acid-base imbalances by adjusting the input speed and concentration of bicarbonate in displacement fluid and modifying bicarbonate-induced alkalization to alleviate hypercapnia. Furthermore, CRRT can rapidly alleviate symptoms of hyperthermia and hypermetabolism in patients with ARDS by using a large amount of low-temperature replacement solution to reduce basal metabolic rate, oxygen consumption, and gas exchange; this alleviation reduces CO_2 production, protects lung function, and avoids ventilation device-related lung injury.[64]

(3) Toxin (Drug) Poisoning

Toxins (drugs) with a large distribution volume in the body (e.g., organophosphorus pesticides, rodenticides, and sleeping pills) are subjected to a secondary distribution mechanism during absorption. They are initially absorbed into the bloodstream, then rapidly transported to tissues. Toxins (drugs) in tissues undergo continuous transfer back into the bloodstream, causing the toxin (drug) concentration to rebound and illness to worsen. Yu *et al*. observed that hemoperfusion combined with CRRT significantly lowered toxin concentrations and removed TNF-α, IL-6, IL-10, and other monocyte-derived cytokines during rodenticide poisoning.[65] For toxins (drugs) with a low relative molecular weight, a low protein-binding rate, and small distribution volume (e.g., methanol and salicylic acid), IRRT initially provides therapeutic benefits and can rapidly reduce the concentrations of toxins (drugs).[66] However, because of its short duration, IRRT is unable to continuously remove toxins and maintain long-term internal environmental homeostasis. For critically ill patients with hemodynamic instability, CRRT can inhibit blood concentration rebound and provide additional benefits.

5 Conclusion

There has been considerable progress in the clinical and technological aspects of CRRT over the last more than 40 years of development. CRRT offers multiple benefits, including hemodynamic stability, rapid re-establishment of homeostasis (e.g., involving electrolytes and acids/bases), and facilitation of nutritional support. It is appropriate as treatment for patients with renal failure, and it provides key support for multiple organ functions. It is important in the treatment of critically ill patients in the ICU, particularly patients with AKI. Currently, there is agreement regarding the need for CRRT in the treatment of critically ill patients; however, engineering-related research concerning the removal mechanisms of CRRT is limited, and there is no comprehensive system for evaluation of filter effectiveness and safety profile. There are also many information gaps in the application of CRRT, such as optimization of filter performance. As a continuously evolving medical technology, CRRT is expected to play a key role in critical care medicine with advances in research and technological innovation, as well as progress in related consumables.

Chapter 2

CRRT Filter Performance: Key Influencing Factors and Indicators

Chapter 2 CRRT Filter Performance: Key Influencing Factors and Indicators

1 Filter Development

The extracorporeal blood circulation system consists of vascular pathways, filters, and blood purification-related devices. The patient's blood flows into the filter through a vascular pathway and indirectly contacts countercurrent dialysate (an aqueous solution containing electrolytes, the osmotic pressure of which is a little higher than the blood). Using the semipermeable membrane principle of the hollow fiber membrane, the accumulated uremic toxins, excess ions, and water in the patient's blood are removed via diffusion, convection, and adsorption; beneficial plasma proteins are retained in the blood. To rectify electrolyte and acid-base imbalances and stabilize the internal environment, ions with low concentrations are substituted by dialysate or replacement solution. Therefore, the most important component of the entire system is the blood purification device that replaces the patient's renal function that is called dialyzer (the treatment of HD), hemofilter (the treatment of HF), diafilter (the treatment of HDF), etc. In this dissertation, we hereafter name the device a "CRRT filter" for the treatment of CRRT because the principal mechanism of mass transfer is "filtration" rather than "diffusion."

In the early 1940s, the Kolff rotating drum dialyzer (developed by Willem Kolff) became the first blood purification device used in a clinical setting.[67] This device comprised a cellophane tubular membrane (inner diameter, 35 mm; length, 30 m) spirally wrapped around a cylinder and transversely inserted into a dialysate-containing tank (Figure 5(a)); the volume of dialysate exceeded one-fourth of the inner diameter of the cylinder. The relatively low resistance of the blood compartment allowed dialysis without a blood pump, but the low hydraulic permeability with very low mechanical strength of the membrane severely limited ultrafiltration; additionally, the maximum volume of the extracorporeal blood compartment was 500–700 mL. The second device to gain widespread acceptance was the Coil dialyzer.[68] This device comprised a cellophane

mesh film (width, 15 cm; length, 4 m) wrapped around the inner wall of the cylindrical housing to achieve high blood compartment pressure through a narrow blood channel; however, this geometry produced a high *TMP*, hindering accurate control of ultrafiltration volume (Figure 5(b)). Subsequently, a Standard Kiil dialyzer with a flat Cuprophan® membrane was developed; this device separated the blood and dialysate in a layer-by-layer manner. Blood flowed between two flat membranes, whereas dialysate flowed between the flat membranes and adjacent separating plates in the opposite direction (Figure 5(c)).[69] Although this design improved the efficiency of diffusion mass transfer, the extracorporeal blood volume remained very large; tunnel effects in the flow paths of blood and dialysate were likely to occur, hindering the maintenance of an equal flow state. In the late 1960s, the introduction of the hollow fiber dialyzer (Figure 5(d)) enabled a decrease in filter volume, reducing the demand for extracorporeal blood compartment capacity, improving blood flow rheology, and significantly increasing dialysis efficiency.[70] Today, most commercially available blood purification devices have hollow fiber structures.

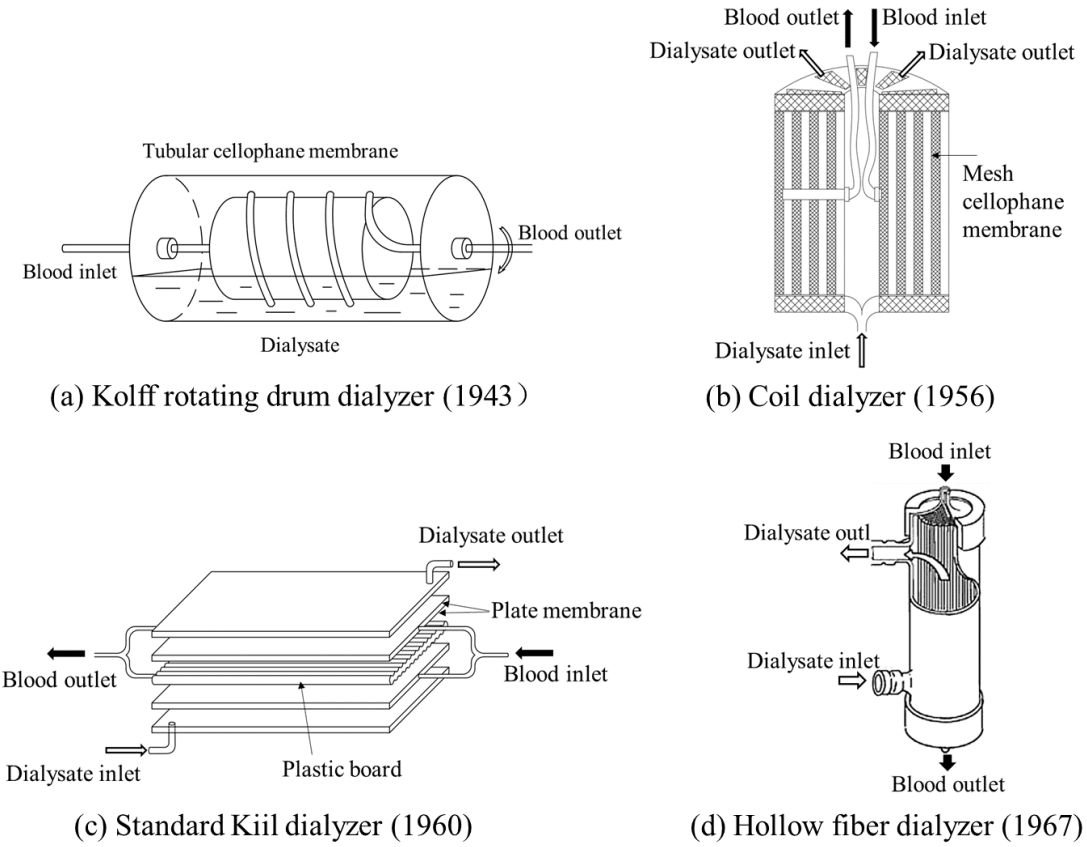

Figure 5. Schematic diagrams of dialysis filters.[71]

A hollow fiber device consists of a hollow fiber membrane bundle and a cylindrical housing. The specifications of the hollow fiber membranes typically include an inner diameter (d) of 200–300 μm, membrane thickness (Δx) of 20–45 μm, and effective hollow fiber length (L) of 160–250 mm.[71] Thousands of hollow fibers are bundled together. When the membrane comes into contact with blood and becomes moist, d, Δx and L must remain largely unchanged; moreover, the membrane material must be light and thin, with high porosity and good mechanical strength. The combination of membrane performance and housing design determines the device effectiveness and safety profile.

CRRT filters have evolved from hollow fiber dialyzers.[72] However, because CRRT has a much smaller Q_D and a relatively larger Q_B (still smaller than that in conventional HD), C_L is limited by Q_D, because C_L never exceeds the smaller value of either Q_B or Q_D. Then CRRT filters must be designed to meet Q_B and Q_D requirements in CRRT. To satisfy the continuous treatment needs of CRRT, the CRRT filter must also efficiently remove low molecular weight proteins (LMWP), while effectively inhibiting the loss of valuable proteins (e.g., albumin).

2 Uremic Toxins and Removal Mechanisms

CRRT is an IRRT-based blood purification system that removes bodily fluids and uremic toxins through the same mechanisms utilized in traditional IRRT: diffusion, convection, and adsorption. Uremic toxins of various molecular weights require distinct removal mechanisms. Uremic toxins with low molecular weights are primarily removed by diffusion, whereas toxins with middle molecular weights and toxins with protein-binding properties are primarily removed by convection or adsorption. Furthermore, removal mechanisms vary among CRRT modes.[50] For example, CVVHD primarily relies on diffusion, CVVH relies on convection, CVVHDF relies on both convection and diffusion, and CPFA relies on both convection and adsorption. Therefore, a comprehensive understanding of the removal mechanisms of various treatment modes, as well as a thorough investigation of the roles of various factors that affect these mechanisms, can provide key insights concerning the optimal treatment mode for patients in various clinical contexts.

2.1 Uremic Toxins

Chronic or acute renal failure can create large amounts of metabolic waste in the body, disrupt homeostatic balance, cause progressive physiological dysfunction in various systems, and eventually lead to death. Uremic toxins are metabolic waste products produced as a result of renal failure. Uremic toxins are classified into three categories according to their physicochemical characteristics and removal modes, as well as clinical outcomes and quality of life indicators (Table 2).[73-74] Low molecular weight uremic toxins (LMs) are water-soluble toxins with a molecular weight of < 0.5 kDa; examples include urea (*MW* = 60 Da), creatinine (Cr, *MW* = 113 Da), and phosphate (P, *MW* = 228 Da). Middle molecular weight uremic toxins (MMs) are water-soluble toxins with molecular weights ranging from 0.5 to 58 kDa; examples include vitamin B_{12} (VB_{12}, *MW* = 1355 Da, although this is not a toxin), β_2-microglobulin (β_2-MG, *MW* = 11.8 kDa), and myoglobin (MB, *MW* = 16.7 kDa). Protein-bound uremic toxins have a molecular weight of < 0.5 kDa, but their high protein-binding rate leads to greater overall molecular weight and difficulty with removal during blood purification; examples include indoleacetic acid (IS, *MW* = 213 Da) and homocysteine (Hcy, *MW* = 135 Da).

Table 2. Categories of uremic toxins.

Class		***MW***	**Biomarker**
LMs	Small molecules	< 0.5 kDa	Urea (60 Da); Cr (113 Da); P (228 Da)
MMs	Small-middle molecules	0.5–15 kDa	VB_{12} (1.4 kDa); β_2-MG (11.8 kDa)
	Medium-middle molecules	15–25 kDa	MB (16.7 kDa)
	Large-middle molecules	25–58 kDa	λ free light chains (45 kDa)
Protein-bound uremic toxins	Protein-bound molecules	Mostly < 0.5 kDa	IS (213 Da); Hcy (135 Da)

MW, molecular weight; LMs, low molecular weight uremic toxins; MMs, middle molecular weight uremic toxins; Cr, creatinine; P, phosphate; VB_{12}, vitamin B_{12}; β_2-MG, β_2-microglobulin; MB, myoglobin; IS, indoxyl sulfate; Hcy, homocysteine.

2.2 Removal Mechanisms

(1) Diffusion

Diffusion is a mass transfer process in which a solute transfers across a semipermeable membrane from a high concentration to a low concentration, eventually producing the same concentration on both sides of the membrane (Figure 6).[75] The driving force of diffusion is the concentration gradient. Thus, a greater difference in solute concentration on either side of the dialysis (semipermeable) membrane facilitates solute diffusion through the membrane and subsequent removal; a smaller difference in solute concentration hinders removal.

During the diffusion mass transfer process, solute transfer is subjected to three layers of mass transfer resistance (Figure 7): the overall resistance (R_o) of a solute to diffusion mass transfer by the filter is equal to the sum of the blood boundary layer mass transfer resistance (R_B), membrane resistance (R_M), and dialysate boundary layer mass transfer resistance (R_D) (equation (1)).[76] The ratio of mass transfer resistance varies according to the removal of toxins with diverse molecular weights (Figure 8).[77] LMs have a smaller molecular radius than membrane pores; their mass transfer resistance is largely concentrated on the blood-dialysate boundary layer and is limited by the stagnant fluid layer in blood-dialysate flow paths. Therefore, the basic principle of improving a filter's diffusion removal performance involves minimizing the boundary layer effect of the membrane. Enhancement of the Q_B can increase wall shear force, may reduce R_B in some extent, and extend the effective area of toxin contact with membranes. Enhancement of the Q_D can improve the dialysate flow state and increase the concentration gradient on either side of the membrane, thereby augmenting diffusion mass transfer. R_M and Δx are positively correlated; therefore, a decrease in Δx can increase diffusion mass transfer. Furthermore, a decrease in d can shorten the dispersion path length and improve diffusion removal efficiency. Because of membrane constraints, the proportion of R_M increases with increasing molecular weight; the diffusion removal efficiency of MMs is limited in conventional (low to medium-flux) membrane.

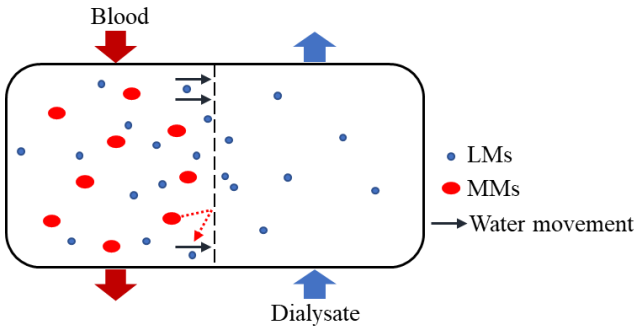

Figure 6. Diffusion mechanism.[75] LMs, low molecular weight uremic toxins; MMs, middle molecular weight uremic toxins.

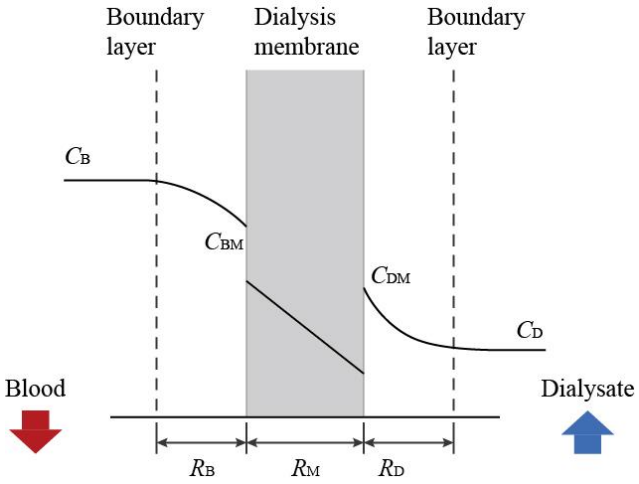

Figure 7. Diffusion mass transfer resistance.[76] R_B, R_M, and R_D, resistances from the blood boundary layer, the membrane itself, and the dialysate boundary layer, respectively; C_B and C_D, solute concentrations on the blood side and the dialysate side, respectively; and C_{BM} and C_{DM}, solute concentrations on the boundary layer of the blood side and the dialysate side, respectively.

$$R_o = R_B + R_M + R_D \quad (1)$$

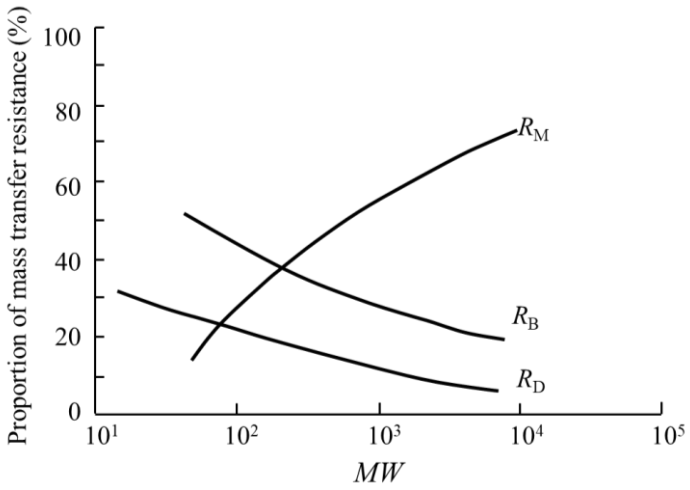

Figure 8. Proportion of mass transfer resistance.[77] *MW*, molecular weight; R_B, R_M, and R_D, resistances from the blood boundary layer, the membrane itself, and the dialysate boundary layer, respectively.

(2) Convection

Convection is a mass transfer process in which the solvent moves from the high-pressure side to the low-pressure side of a semipermeable membrane under a gradient of osmotic or hydrostatic pressure, and the solute also moves through the semipermeable membrane (Figure 9).[75] Transmembrane pressure (*TMP*), the driving force of convection, is created by the pressure gradient formed on either side of the membrane. Transmembrane ultrafiltration occurs when *TMP* causes water in the blood to flow from the blood side to the dialysate side; specific molecular weight solutes are also removed in this process.[78]

Membrane characteristics have a significant impact on convective removal performance.[79] Key parameters influencing membrane characteristics include membrane pore size, porosity, pore structure, maximum molecular weight rejection, and membrane surface charge. For a specific membrane area, increases in membrane pore size and porosity can improve solute and hydraulic permeabilities of the membrane. The effects of pore structure are more complex; pore length and regularity can alter the molecular weight retention size, thereby influencing membrane filtration performance. The membrane surface charge also has a significant impact because most plasma proteins are larger than the membrane pore size and are intercepted by the membrane during

ultrafiltration; these properties contribute to concentration polarization and membrane fouling. Although concentration polarization and membrane fouling have distinct mechanisms of action, both can cause an increase in the mass transfer resistance of the membrane, thereby reducing convective mass transfer efficiency. A moderate negative charge on the membrane surface can diminish the impact of the membrane on proteins, inhibiting concentration polarization and membrane fouling.

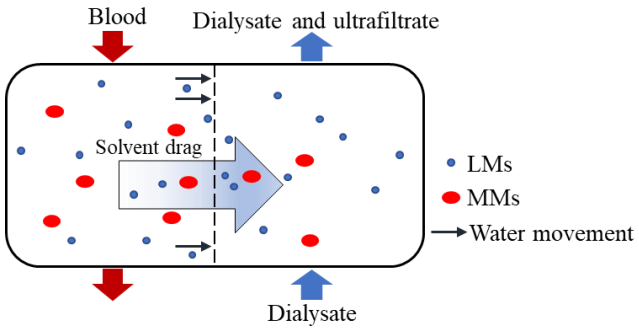

Figure 9. Convection mechanism.[75] LMs, low molecular weight uremic toxins; MMs, middle molecular weight uremic toxins.

(3) Adsorption

Adsorption is the formation of microporous adsorbent structures according to the molecular chemical structure and polarization of the adsorbent material, with distinct functional groups on the surface. Because of intermolecular forces or interactions between positive and negative charges, an adsorbent exhibits adsorption performance on specific solutes (Figure 10).[75] The adsorption and removal efficiency of a filter for a specific solute can be improved in a targeted manner by selecting a membrane with appropriate pore size distribution and adsorption characteristics according to toxin molecular weight, chemical structure, and biological properties. For example, hydrophobic groups on the surface of some membranes can selectively adsorb proteins, drugs, and toxic chemicals (e.g., β_2-MG, complement, and endotoxin); other membranes exhibit antigens and antibodies on the surface, enabling the use of biological affinity to specifically adsorb corresponding antibodies and antigens in the blood.

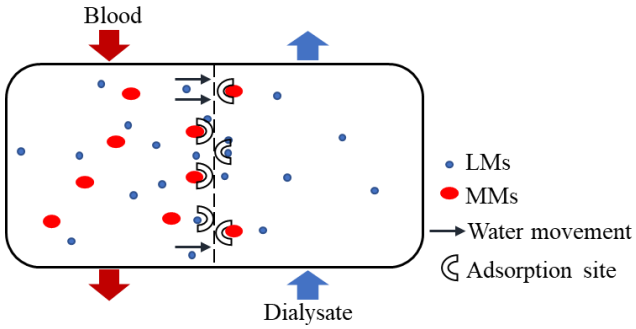

Figure 10. Adsorption mechanism.[75] LMs, low molecular weight uremic toxins; MMs, middle molecular weight uremic toxins.

3 Performance Evaluation Indicators

The core technical concept of blood purification involves the use of a blood purification device to transfer and remove water, electrolytes, and solutes from the blood, then return the purified blood to the human body to ensure internal environmental balance. The selection of an appropriate device is extremely important for therapeutic efficacy; therefore, qualified technical indicators are needed to evaluate device performance. The international standard ISO 8637-1:2017 proposes many important indicators for evaluation of device performance.[80]

3.1 Clearance (C_L)

C_L, which represents the removal of a solute from blood expressed as volume per unit time, is an important index for evaluating the solute removal performance of the blood purification device. C_{BI} and C_{BO} are the sample concentrations at the blood inlet and outlet, Q_{BI} and Q_{BO} are the blood flow rates at the inlet and outlet of the device, respectively. Assuming that ultrafiltration does not occur during dialysis (i.e., filtrate flow rate (Q_F) = 0 mL/min), then $Q_{BO} = Q_{BI}$. The residual dissolved mass of a given solute after removal by a filter is $(Q_{BI} - C_L) \times C_{BI}$, which is consistent with the equivalent value of $Q_{BI} \times C_{BO}$ according to the law of conservation of matter (i.e., equation (2)).

$$C_{\mathrm{L}} = \left(\frac{C_{\mathrm{BI}} - C_{\mathrm{BO}}}{C_{\mathrm{BI}}}\right) Q_{\mathrm{BI}} \qquad (2)$$

Assuming that ultrafiltration occurs (i.e., Q_F > 0 mL/min), then $Q_{BO} = Q_{BI} - Q_F$. In this case, $(Q_{BI} - C_L) \times C_{BI}$ and $Q_{BO} \times C_{BO}$ are equal. Therefore, C_L is represented by equation (3).

$$C_{\mathrm{L}} = \frac{Q_{\mathrm{BI}} C_{\mathrm{BI}} - Q_{\mathrm{BO}} C_{\mathrm{BO}}}{C_{\mathrm{BI}}} = \left(\frac{C_{\mathrm{BI}} - C_{\mathrm{BO}}}{C_{\mathrm{BI}}}\right) Q_{\mathrm{BI}} + \frac{C_{\mathrm{BO}}}{C_{\mathrm{BI}}} Q_{\mathrm{F}} \qquad (3)$$

3.2 Overall Mass Transfer Membrane Area Coefficient (K_oA) and Dialysis Efficiency (E)

The following discussion is specifically applied for a blood purification device called the dialyzer with no ultrafiltration. For a given solute, the C_L by the dialyzer is related to the mass transfer coefficient and effective membrane area (A). The mass transfer coefficient, defined as the reciprocal of mass transfer resistance, represents the difficulty of mass transfer. According to equation (1), the overall mass transfer coefficient (K_o) can be expressed by equation (4) (Figure 11).

$$\frac{1}{K_{\mathrm{o}}} = \frac{1}{K_{\mathrm{B}}} + \frac{1}{K_{\mathrm{M}}} + \frac{1}{K_{\mathrm{D}}} \qquad (4)$$

where K_B, K_M, and K_D are mass transfer coefficients of the blood boundary layer, the membrane itself, and the dialysate boundary layer, respectively.

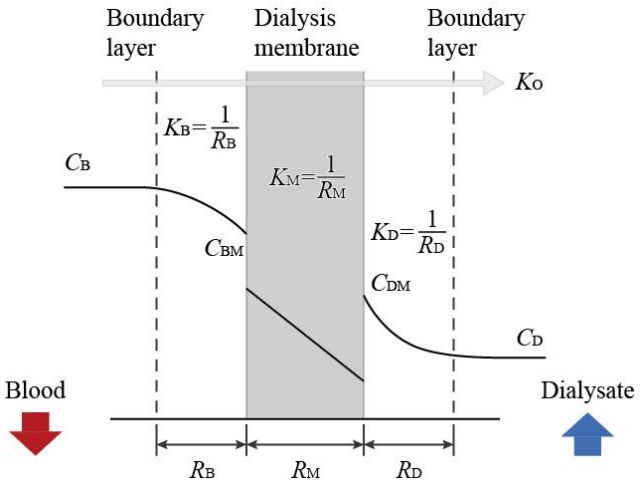

Figure 11. Mass transfer coefficients. K_o, overall mass transfer coefficient; K_B, K_M, and K_D, mass transfer coefficients of the blood boundary layer, the membrane itself, and the dialysate boundary layer, respectively; R_B, R_M, and R_D, resistances from the blood boundary layer, the membrane itself, and the dialysate boundary layer, respectively; C_B and C_D, solute concentrations on the blood side and the dialysate side, respectively; and C_{BM} and C_{DM}, solute concentrations on the membrane surface in boundary layer of the blood side and that of the dialysate side, respectively.

According to the law of conservation of mass, the decrease in solute on the blood side is equal to the increase in solute on the dialysate side. Thus, the mass transfer rate ($\dot{m}$) equals:

$$\dot{m} = Q_B(C_{BI} - C_{BO}) = Q_D(C_{DO} - C_{DI}) \qquad (5)$$

$\dot{m}$ can also be determined by the overall mass transfer area coefficient (K_oA), a combined parameter consisting of K_o, effective surface area A, and $(C_B - C_D)_{av}$, which signifies the mean difference in solute concentration between the blood and the dialysate.

$$\dot{m} = K_oA(C_B - C_D)_{av} \qquad (6)$$

$(C_B - C_D)_{av}$ refers to the logarithmic concentration difference (equation (7)); 'ln' is an abbreviation for the natural logarithm.

$$(C_B - C_D)_{av} = \frac{(C_{BI} - C_{DO}) - (C_{BO} - C_{DI})}{\ln\left(\frac{C_{BI} - C_{DO}}{C_{BO} - C_{DI}}\right)} \qquad (7)$$

According to the preceding equations, C_L can be represented by the functional relationship among Q_B, Q_D, A, and K_o (equation (8)).[81] The K_oA (equation (9)) derived from equation (8) is

also measured in volume per unit time, reflecting the permeability of the dialyzer to a given solute; it can be regarded as the potential removal performance of the dialyzer, which is used to analyze the diffusion effectiveness of the dialyzer quantitatively.

$$C_{\mathrm{L}} = Q_{\mathrm{B}} \left[\frac{\exp\left(\frac{K_{\mathrm{o}}A(1 - Q_{\mathrm{B}}/Q_{\mathrm{D}})}{Q_{\mathrm{B}}}\right) - 1}{\exp\left(\frac{K_{\mathrm{o}}A(1 - Q_{\mathrm{B}}/Q_{\mathrm{D}})}{Q_{\mathrm{B}}}\right) - Q_{\mathrm{B}}/Q_{\mathrm{D}}} \right] \tag{8}$$

$$K_{\mathrm{o}}A = \frac{Q_{\mathrm{B}}}{1 - \frac{Q_{\mathrm{B}}}{Q_{\mathrm{D}}}} \ln\left(\frac{1 - \frac{C_{\mathrm{L}}}{Q_{\mathrm{D}}}}{1 - \frac{C_{\mathrm{L}}}{Q_{\mathrm{B}}}}\right) \tag{9}$$

For a given solute, C_{L} by a dialyzer is correlated with Q_{B}.[68] When the Q_{D} is constant, C_{L} exhibits a linear relationship with the Q_{B}. When the Q_{B} exhibits an infinite increase and solute concentrations in the dialysate and blood approach equilibrium, the relationship curve between C_{L} and Q_{B} forms a plateau, indicating that the limiting region of $K_{\mathrm{o}}A$ has been reached. Thus, a larger $K_{\mathrm{o}}A$ implies that a greater Q_{B} is required to reach this plateau. There is a similar relationship between the Q_{D} and the diffusion clearance for a given solute; accordingly, $K_{\mathrm{o}}A$ can be regarded as the maximum C_{L} that a dialyzer can obtain under specific flow conditions, implying that solute removal performances of the dialyzer for middle and high molecular weight solutes are mainly limited by $K_{\mathrm{o}}A$. The minimum values of Q_{B}, Q_{D}, and $K_{\mathrm{o}}A$ determine the overall removal performance of a dialyzer.[82]

The arithmetic definition of the membrane surface area, A_{o}, is calculated by equation (10).[83]

$$A_{\mathrm{o}} = \pi dLN \tag{10}$$

where N is the number of hollow fibers.

The value defined by the above equation, however, may usually be different from the effective surface area, A, the area where the diffusion really occurs with no obstructions. Also, although a particular dialyzer has a set value for the $K_{\mathrm{o}}A$, optimization of the housing design can theoretically improve the $K_{\mathrm{o}}A$ of the dialyzer. For specific values of Q_{B} and Q_{D}, R_{M} can be reduced by decreasing the Δx, thereby increasing the $K_{\mathrm{o}}A$ of the dialyzer. Furthermore, spacers can be added to the hollow fiber membrane bundle or designed with microwave structures to maximize the improvement of dialysate and blood perfusion, increase A (not A_{o}), and enhance the $K_{\mathrm{o}}A$ of the dialyzer.

N_{T}, the number of transfer unit, is a direct measure of transmembrane mass transfer efficiency

(equation (11)), such that higher N_T values are associated with greater mass transfer efficiency per unit flow rate. Z is the blood flow to dialysate flow ratio (equation (12)). By substituting equations (11) and (12) into equation (8), an equation for calculation of dialysis efficiency (E) can be constructed (equation (13)). E represents the maximum solute removal fraction that the dialyzer can actually achieve.

$$N_{\mathrm{T}} = \frac{K_{\mathrm{o}}A}{Q_{\mathrm{B}}} \tag{11}$$

$$z = \frac{Q_{\mathrm{B}}}{Q_{\mathrm{D}}} \tag{12}$$

$$E = \frac{C_{\mathrm{L}}}{Q_{\mathrm{B}}} = \frac{1 - \exp[N_{\mathrm{T}}(1 - z)]}{z - \exp[N_{\mathrm{T}}(1 - z)]} \tag{13}$$

3.3 Internal Filtration Flow Rate (Q_{IF})

Blood flows on the inside of the hollow fiber membrane; dialysate flows countercurrently or in the opposite direction to the blood stream on the outside of the membrane. On blood and dialysate sides, the pressure is skewed in opposite directions (Figure 12).[84] At the blood inlet, pressure is higher on the blood side than on the dialysis side, and the positive *TMP* induces the forward filtration or the water transport from the blood compartment toward the dialysate compartment, whereas the negative *TMP* induces the backward filtration or the water transport from the dialysate compartment to the blood compartment because the pressure is higher on the dialysate side than on the blood side. Figure 12 illustrates how a pressure drop on the dialysate and blood sides increases the *TMP* at any point in the dialyzer/filter, improving mass transport by convection. Integrated forward and backward filtration occurring in one blood purification device at the same time in the different region is called “internal filtration.”

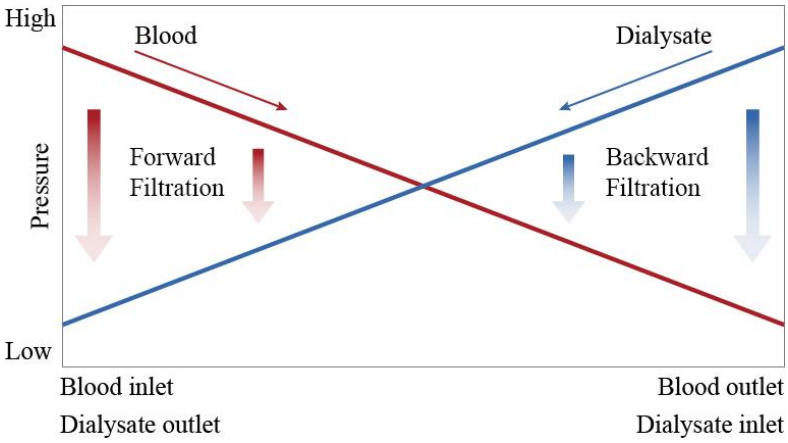

Figure 12. Schematic of pressures during internal filtration.[84]

High-flux membrane device undergo substantial positive (forward) and negative (backward) filtration (i.e., internal filtration).[84] Sato *et al.* used Doppler ultrasonography to measure the maximum internal filtration flow rate ($Q_{IF\text{-}Max}$) accurately in high-flux dialyzers.[85] The detection device for internal filtration flow rate (Q_{IF}) measurement is shown in Figure 13. A Doppler ultrasonography with a pulse-wave of 7.5 MHz was used to measure blood velocity at various points along the direction of blood flow. In this method, $Q_{IF\text{-}Max}$ (equation (15)) is calculated as the difference between the inlet blood flow rate (Q_{BI}) and the minimum blood flow rate (Q_{BM}).

$$S = \frac{1}{4} N\pi L^2 \qquad (14)$$

$$Q_{IF-Max} = Q_{BI} - Q_{BM} = V_{BI}S - V_{BM}S \qquad (15)$$

where S is the cross-sectional area of the hollow fibers, V_{BI} is the inlet blood flow velocity, and V_{BM} is the minimum blood flow velocity.

Sakiyama *et al.* used this method to measure the $Q_{IF\text{-}Max}$ of high-flux polysulfone (PSf) membrane dialyzers; the results showed that at the Q_B of 350 mL/min, the $Q_{IF\text{-}Max}$ could reach 58 mL/min; this was twofold higher than the $Q_{IF\text{-}Max}$ when the Q_B was 200 mL/min. The internal filtration enhanced the convection effects, increasing the C_L for β_2-MG by approximately 20%.[86] The promotion of internal filtration can enhance the convection effects, thereby improving the effectiveness of middle and high molecular weight solute removal. Accordingly, measurements of the Q_{IF} effectively quantify the extent of transmembrane water movement caused by the blood purification device (i.e., convection effects).

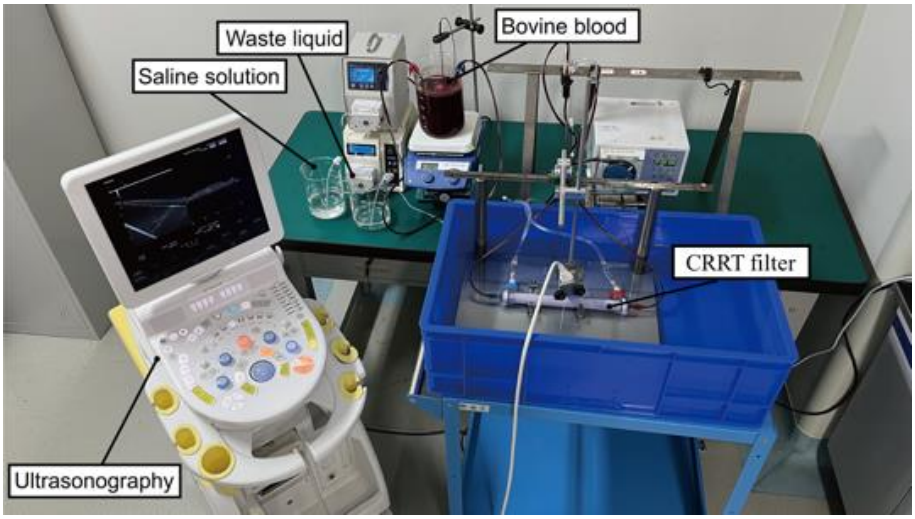

Figure 13. Internal filtration flow rate measurement system.

In accordance with the principles of the Hagen–Poiseuille equation,[84] pressure drops on the blood side and the dialysate side are calculated by equations (16) and (19), respectively. Mineshima *et al.* demonstrated that reasonable optimization of design factors can significantly increase Q_{IF}.[87] Decreasing d or increasing L leads to an increase in pressure drop on the blood side, thereby promoting Q_{IF}. An increase in hollow fiber packing density (PD) narrows the dialysate flowable space and increases the pressure drop on the dialysate side, thus promoting Q_{IF}. However, increasing the pressure drop on the blood side or dialysate side may lead to the risks of hemolysis and membrane rupture. Therefore, d, L, and PD must be designed within a reasonable range.

$$\Delta P_{\mathrm{B}} = P_{\mathrm{BI}} - P_{\mathrm{BO}} = \frac{128\mu_{\mathrm{B}} L Q_{\mathrm{B}}}{N\pi d^4} \tag{16}$$

$$D_{\mathrm{e}} = \frac{D^2 - (d + \Delta_{\mathrm{x}})^2 N}{(d + \Delta_{\mathrm{x}})N} \tag{17}$$

$$S_{\mathrm{D}} = \frac{\pi[D^2 - (d + \Delta_{\mathrm{x}})^2 N]}{4} \tag{18}$$

$$\Delta P_{\mathrm{D}} = P_{\mathrm{DI}} - P_{\mathrm{DO}} = \frac{32\mu_{\mathrm{D}} L Q_{\mathrm{D}}}{{D_{\mathrm{e}}}^2 S_{\mathrm{D}}} \tag{19}$$

where ΔP_{B} and ΔP_{D} are pressure drops on the blood side and dialysate side, respectively; P_{BI}, P_{BO}, P_{DI}, and P_{DO} are the inlet and outlet pressures on the blood side and the inlet and outlet pressures on the dialysate side, respectively; μ_{B} and μ_{D} are the viscosities of the blood and dialysate, respectively; D_{e} is the equivalent diameter of the dialysate flow path; and S_{D} is the cross-sectional area of the dialysate flow path.

3.4 Transmembrane Pressure (*TMP*) and Ultrafiltration Coefficient (k_{UF})

TMP is the overall pressure difference on either side of the membrane, calculated by subtracting filtrate pressure (P_F) from the mean of the inlet pressure (P_{BI}) and outlet pressure (P_{BO}) of the blood side (equation (20)).

$$TMP = \frac{P_{BI}+P_{BO}}{2} - P_F \qquad (20)$$

Because of concentration polarization and membrane fouling within the device, the *TMP* in general increases with time in any kind of blood purification therapy, including CRRT. Water removal is an important objective of CRRT; it is most often accomplished through ultrafiltration, which is governed by the *TMP*. During the ultrafiltration process, solutes with high relative molecular weight are intercepted by the membrane because of the membrane pore size, resulting in concentration polarization on the membrane surface.[88] The rapid formation of a concentration polarization layer results in a rapid decrease in membrane filtration efficacy and an increase in convective mass transfer resistance. Especially in the early stages of treatment, the concentration polarization layer rapidly increases, and the *TMP* rapidly increases to meet the set Q_{UF}. Furthermore, membranes cause non-specific adsorption of high molecular weight solutes such as plasma proteins; this process results in solute deposition on the membrane surface or within membrane pores, blockage of membrane pores, and membrane fouling. The thickening of the formed filter cake layer is also an important factor in reducing the membrane filtration efficacy, which also can increase convective mass transfer resistance. The initial membrane fouling is relatively mild, allowing passage of some fluids. As the duration of treatment increases, additional high molecular weight solutes flow to the membrane surface or pores, increasing the flow resistance through each blocked area and aggravating membrane fouling. This process results in a continual increase in the *TMP*, which reaches a critical value upon membrane fouling saturation.

The *TMP* has a direct impact on filter effectiveness and safety profile. Convection requires a *TMP* gradient to cause fluid motion.[89] If the permeation flux increases with increasing *TMP* during ultrafiltration, the corresponding pressure range is regarded as the pressure-dependent zone (i.e., the area where the membrane performs the best and the convection effect is enhanced). If the permeation flux does not increase in a linear manner with *TMP*, the membrane reaches fouling

saturation, and the removal performance of the device is diminished. Extracorporeal blood circulation typically functions at a constant ultrafiltration flow rate, rather than a constant *TMP*, to reduce the negative effects of concentration polarization and membrane fouling; the *TMP* is increased to maintain constant ultrafiltration flux.[90] However, large fluctuations in *TMP* are likely to cause abrupt changes in osmotic pressure and worsen a patient's hemodynamic instability. Furthermore, excessive *TMP* can damage red blood cells and denature proteins, resulting in cell membrane stretching and rupture, membrane pore deformation, and significant protein loss. Therefore, minor variations in *TMP* are critical safety profile indicators when designing CRRT filters. The *TMP* must remain stable within a specific range, maintain hemodynamic stability, inhibit excessive protein loss, and support enhancement of convection effects and optimization of solute removal efficiency.

The ultrafiltration coefficient, k_{UF}, is an indicator that quantifies a hydraulic permeability of the device, defined by the following equation (21), i.e.,

$$k_{\mathrm{UF}} = \frac{Q_{\mathrm{UF}}}{TMP} \qquad (21)$$

This value is sometimes called *UFR* (ultrafiltration rate) in clinical situations; however, this naming is not preferred especially when membrane performance is discussed because "ultrafiltration rate" also refers to the "rate of ultrafiltration", Q_{UF}. A gradual decline in k_{UF} during CRRT always be a useful measure of the effectiveness and lifetime of the filter.

3.5 Concentration Polarization Mass Transfer Resistance (R_c)

Concentration polarization refers to the phenomenon that solutes with a high molecular weight (e.g., most plasma proteins) are intercepted by the membrane and highly concentrated near the membrane surface; this ultimately results in the formation of a concentration polarization layer (Figure 14).[88]

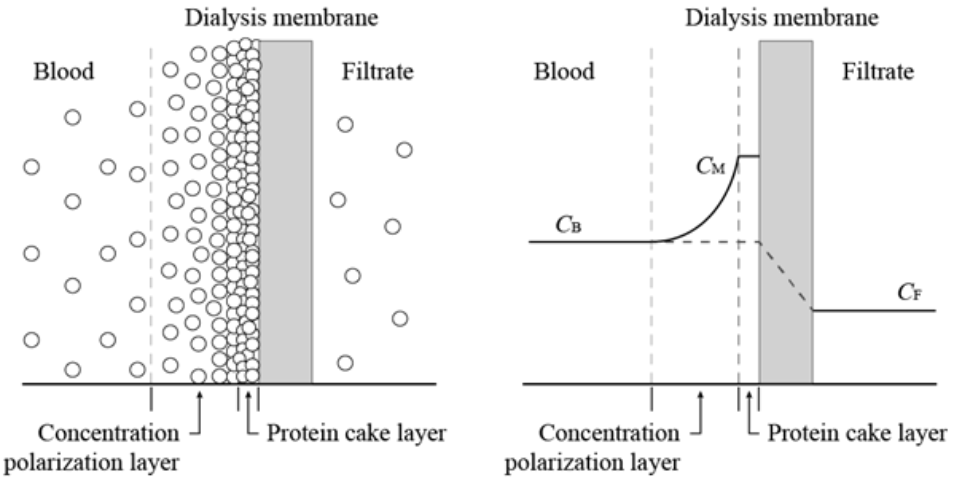

Figure 14. Schematic of concentration polarization.[88]

Concentration polarization is an important indicator of protein filtration, which indirectly reflects the safety profile of the filter. When concentration polarization occurs, the protein concentration is significantly greater in the concentration polarization layer than in the bulk solution; moreover, the extent of protein filtration is enhanced in the concentration polarization layer.[91] Importantly, a decrease in concentration polarization layer formation leads to less filtration of beneficial proteins (e.g., albumin), thus improving the safety profile of the filter.[92] Concentration polarization mass transfer resistance (R_c) can be used to quantitatively evaluate concentration polarization layer formation; a larger R_c indicates a thicker concentration polarization layer.[93]

In terms of the increase in mass transfer resistance caused by solute accumulation on the membrane surface or pores, the total mass transfer resistance (R_t) includes the mass transfer resistance caused by R_m, R_c, and the mass transfer resistance caused by the protein cake layer (R_f) (equation (22)).[93] The R_t is computed by dividing the TMP_1 at a given operating time by the permeation flux (J) and filtrate viscosity of the membrane (μ) (equation (23)).

$$R_t = R_f + R_m + R_c \quad (22)$$

$$R_t = \frac{TMP_1}{J \cdot \mu} \quad (23)$$

Because of the reversibility of mass transfer resistance caused by the concentration polarization layer, a TMP_2 that minimizes the influence of concentration polarization can be obtained by fully flushing the blood side with buffer solution and conducting pressure testing; R_f +

R_m can then be calculated (equation (24)). Equations (22)-(24) can be used to calculate the R_c value.

$$R_f + R_m = \frac{TMP_2}{J \cdot \mu} \quad (24)$$

3.6 Sieving Coefficient (*SC*)

SC, an important evaluation indicator of solute removal through convection effects, is used to describe the potential of different solutes to pass across a particular membrane.[94] Although there are so many definitive equations of the sieving coefficient, *SC* in this dissertation was calculated by equation (25) at each time point using the protein concentration of the filtrate (C_F), C_{BI}, and C_{BO}.

$$SC = \frac{2C_F}{C_{BI} + C_{BO}} \quad (25)$$

A larger *SC* value for removal of the target solute indicates stronger filtration efficacy for that solute. However, the *SC* value for non-removal target solutes (e.g., albumin) must be maintained within a specific range to avoid causing nutritional imbalance, and other complications. Formation and development of a concentration polarization layer and a protein cake layer often cause changes in filtration efficacy during the treatment process. Therefore, the efficacy of the filter can be evaluated by monitoring changes in *SC* over time; this indicator can also be used to evaluate albumin filtration performance, thus predicting the filter safety profile.

3.7 Amount of Albumin Filtered (M_{fld})

The amount of albumin filtered (M_{fld}) is an important indicator of a safety profile of the filter. It can be quantified by continuously measuring the albumin concentration in the filtrate and was calculated as an area under the curve of the rate of mass filtration, Q_F x C_F (equation (26)).[95]

$$M_{fld} = \int_0^t Q_F \, C_F dt \quad (26)$$

Albumin is the most abundant protein in plasma, comprising more than 50% of all serum proteins[96]; it plays a prominent role in the maintenance of stable plasma colloid osmotic pressure[97].

The use of high-flux membranes during CRRT may cause nutrient loss, negatively impacting the patient's nutritional status. The primary goal of CRRT is maintenance of the patient's hemodynamic stability; albumin filtration must be strictly controlled to optimize the overall safety profile. M_{fld} is used to quantitatively evaluate albumin retention characteristics of the membrane to assure safety profile of the filter.

4 CRRT Filter Design

CRRT filter performance depends on membrane permeability to water and solutes, along with design factors. The membranes currently used in CRRT filters display a design that is nearly identical to the design of hollow fiber membranes. Despite their origins in chronic blood purification, current filters have been continuously developed and now meet CRRT performance requirements for biocompatibility, permeability, and toxin removal. In terms of housing, most designs adhere to dialyzer housing conventions; there remains considerable potential for improvements in design factors such as effective hollow fiber length (L) and inner housing diameter (D), the ratio of L to D (L/D ratio), as well as hollow fiber packing density (PD).

4.1 Membranes for CRRT

The implementation of membrane separation technology in medicine has led to significant advancements in human life sciences. The most important component of extracorporeal blood purification therapy is the membrane, which serves as the separation medium. The spinnability of the membrane material is a key consideration in the fabrication of membranes via dissolution, extrusion, and film formation processes. Membranes for various blood purification treatments must have high mechanical strength, good water and solute permeability, disinfectant properties, and excellent biocompatibility. Membranes for conventional dialysis have advanced through four stages of development: natural cellulose, modified cellulose, synthetic polymers, and optimization from low flux to high flux. The materials currently used as clinical dialysis membranes are classified into two categories, i.e., natural polymers and synthetic polymers.

(1) Natural Polymer Membranes

Early dialysis membranes consisted of natural cellulose; their basic structure and thin membrane thickness (6–12 mm) were conducive to diffusion mass transfer. However, the inherent low permeability of plant fibers limited the use of such membranes in convection therapy. Furthermore, unmodified regenerated cellulose membranes exhibited many biocompatibility issues, such as acute leukopenia and complement activation.[98-99] A series of improvement studies led to the development of various modified cellulose membranes. The membrane pore sizes were increased, adverse effects (e.g., inflammation) were reduced, and the MM flux and removal performances were improved. In particular, a later version of cellulose triacetate membranes demonstrated good therapeutic effects when used in clinical settings.[100] Pichaiwong *et al.* used a modified cellulose triacetate membrane in CRRT; this approach considerably resolved difficulties such as complement activation and achieved biocompatibility similar to the compatibility of PSf membrane.[101]

(2) Synthetic Polymer Membranes

Synthetic polymer membranes (e.g., polyacrylonitrile (PAN), polymethyl methacrylate (PMMA), and PSf) were presented in the late 1970s.[102] The membrane thickness (Δx) of an early synthetic polymer membrane was approximately 100 μm. It was only appropriate for hemofiltration because it did not support diffusion mass transfer. After modification, the Δx was considerably reduced and the membrane structure was optimized. In contrast to cellulose membranes, synthetic polymer membranes can be constructed as asymmetric membranes with dense inner surfaces and porous support structures. They have superior mechanical strength, higher porosity, better permeability and biocompatibility, and more robust capacity to reproduce the natural filtration functions of the kidneys.

In 1985, β_2-MG was identified as a factor associated with carpal tunnel syndrome in long-term dialysis patients.[103] Since then, extensive clinical research has revealed that low relative molecular weight proteins, such as β_2-MG, cannot be completely removed by low-flux membranes. The removal of such proteins requires membranes with sufficient pore size, high permeabilities

both for fluid and solutes of interest. Simultaneously, to avoid the loss of beneficial proteins in the body and corresponding negative effects on patient prognosis, membranes require a reasonable mean pore size distribution. By adjusting the membrane manufacturing process to modify the pore size and pore size distribution, researchers created a series of high-flux synthetic polymer membranes with large pore sizes. The typical membrane pore size is 2.9–3.5 nm, and the k_{UF} > 20 mL/(hr·mmHg).[104] Dialyzers used in chronic blood purification are usually classified either in low-flux or in high-flux mainly depending on the filtration performance. Because CRRT filters exclusively use high-flux membranes with high permeability to water and solutes, above mentioned classification is less appropriate for CRRT filters. When evaluating membranes for CRRT filters, k_{UF} > 20 mL/(hr·mmHg) is an appropriate criterion.

CRRT requires long-term anticoagulation management, typically using intravenous heparin as an anticoagulant to promote biocompatibility; however, this approach can exacerbate adverse effects such as bleeding and heparin-induced thrombocytopenia.[105] Ren *et al.* used a covalent bond to adhere heparin to the PSf membrane surface.[106] The modified membrane exhibited improved hydrophilic properties, prolonged clotting time, and reduced platelet adherence. Moreover, the membrane demonstrated a local anticoagulant effect and could minimize the requirement for heparin during treatment. Similarly, Hirayama *et al.* used heparin to modify the membrane surface of AN69 membrane (a copolymer of acrylonitrile and sodium methallylsulfonate, a highly negatively charged membrane); this yielded the AN69-ST membrane (AN69 with positively charged polyethylene imine, a membrane with reduced negative charge), which demonstrated good anticoagulant performance and could be specifically used for CRRT.[107] Furthermore, CRRT requires the use of filters to actively remove inflammatory mediators from the patient's body and re-establish a stable immune response. Stasi *et al.* showed that PMMA membranes can significantly reduce tissue and systemic complement activation, restrict renal damage and fibrosis, and improve overall inflammatory status; thus, the membranes are appropriate for CRRT.[108]

4.2 Design Factors

Design factors include all design parameters that affect the effectiveness and safety profile of

filters, such as *d*, *Δx*, *L*, *N*, *A*, *D*, *PD*, a baffle structure near the dialysate inlet and outlet, and a taper structure at both ends of the housing. The geometric characteristics of dialyzers/filters are closely related to their performances; therefore, improvements in filter performance require the optimization of all the design parameters.

(1) Baffle Structure and Taper Structure

The performance of a filter greatly depends on blood and dialysate flow conditions.[109] To maximize the mass transfer rate between blood and dialysate, dialysate must flow uniformly within the dialyzer and travel directly to the end of the dialyzer. To achieve this flow pattern, a baffle structure is installed at the inlet and outlet of the dialysate, or a taper structure is installed at both ends of the housing (Figure 15); these structures guide the dialysate into and out of the dialyzer, thereby optimizing dialysate flow. Fukuda *et al.* conducted computer simulation to investigate the impact of housing with or without a taper structure on the flow of dialysate into a hollow fiber membrane bundle; they found that the taper structure was associated with radial fluid dynamics.[110] The reduction of radial fluid force in housing without a taper structure hinders dialysate flow into the central area of the membrane bundle, thereby reducing diffusion removal efficiency; in housing with excess taper length, the increase in fluid volume on the dialysate side and the decrease in dialysate linear velocity can also reduce diffusion removal efficiency. To further explore the optimal design of baffle structures and the optimal length range of taper structures, Yamamoto *et al.* used computer simulation to systematically analyze the impacts of baffle structures and taper structures (i.e., taper angle and taper length) on dialysate flow.[111] A fully enclosed baffle and moderate taper design have been identified as key factors in the free and uniform flow of dialysate into the hollow fiber membrane bundle; they can achieve efficient dialysate distribution in the membrane bundle, effectively reduce dead corners during mass transfer, increase A_o, and improve device effectiveness. The optimal ranges of taper angle and taper length are 2–4 °and 12.5–25.0 mm, respectively for dialyzers used for conventional dialysis therapy.

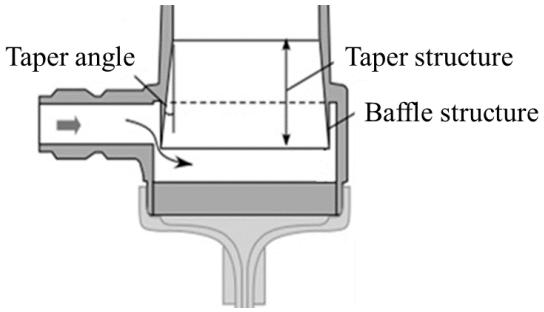

Figure 15. Schematic diagram of baffle structure and taper structure.[110]

(2) Inner Diameter (*d*) and Effective Length (*L*) of Hollow Fiber

Although baffle and taper structures can effectively supply dialysate into the membrane bundle, Hirano *et al.* used a pulse response method to evaluate the flow rates of blood and dialysate; they found that *d*, *L*, and *PD* had greater impacts on fluid flow inside the hollow fiber device.[112] Nguyen *et al.* investigated their impacts on effectiveness by designing a series of hollow fiber devices with various *d*; the results showed that a strict control of key design parameters (e.g., *d* and Δx) was necessary to improve the removal performance for low to middle molecular weight and protein-bound uremic toxins.[113] By comparing the performances of two dialyzers (d = 175 μm and 200 μm), Ronco *et al.* discovered that a decrease in *d* can enhance the blood pressure drop, increase *TMP* at the proximal end and negative pressure at the distal end of the dialyzer, and promote internal filtration, thereby improving removal performance for MMs such as VB_{12}.[114] Using a model design and experimental methodologies, Raff *et al.* showed that, in the presence of constant *PD*, a decrease in *d* and concurrent increase in *L* could significantly improve toxin removal performance.[115] Furthermore, Sato *et al.* also evaluated the impact of *L* on the performance in a clinical setting.[116] When *d* and A_o were constant, an increase in *L* resulted in a significant change in pressure drop along the length of the dialyzer, thereby enhancing internal filtration and improving toxin removal performance.

(3) Hollow Fiber Packing Density (*PD*)

The solute removal efficiency of the device is heavily influenced by the flow distribution of

blood and dialysate.[109] If the filter design results in uneven distribution of blood flow inside the membrane or tunneling effects in the dialysate flow pathway outside of the membrane, removal efficiency may be significantly reduced. *PD*, defined as the ratio of the cross-sectional area of the membrane bundle to that of outer casing with the inner diameter *D* (equation (27)), is an important design factor that affects flow distribution and filter effectiveness.

$$PD = \left(\frac{d+2\Delta x}{D}\right)^2 N \qquad (27)$$

The blood flow rate outside of the membrane bundle is lower than the rate among hollow fibers in the central region of the membrane bundle; the flow of dialysate is subject to relatively high resistance in the central region of the membrane bundle, whereas resistance in the periphery is relatively low. Accordingly, dialysate flows more rapidly in portions of the filter with lower blood flow velocity. A high *PD* hinders dialysate injection into the membrane bundle, resulting in reduced removal efficiency; in contrast, a low *PD* causes a tunnel effect, reducing dialysate utilization and resulting in insufficient solute removal. To increase peripheral blood flow velocity and reduce the risk of coagulation in peripheral fibers, Ronco *et al.* placed an "O" ring around the membrane bundle in the middle of the dialyzer.[117] Hirano *et al.* reported that *PD* values between 48% and 67% allowed both blood and dialysate to freely enter the device, increasing the contact area between blood and dialysate; these *PD* values increased the solute clearance efficiency of a dialyzer for conventional dialysis.[118] Donato *et al.* demonstrated that increasing *PD* to 55%–60% could facilitate optimal dialyzer design while considering manufacturing feasibility and the maximum mechanical stress that red blood cells can tolerate.[119]

(4) Ratio of Effective Length (*L*) to the Inner Diameter (*D*) of the Housing (*L*/*D* Ratio)

The *L*/*D* ratio, which determines the housing shape of the device, is defined as the ratio of effective length to the inner diameter of the housing or the outer casing of the device. The housing shape directly affects the flow of blood and dialysate, thereby influencing mass transfer. Suzuki *et al.* attempted to model filters using the Hagen–Poiseuille equation and Blake–Kozeny equation; subsequently, they conducted computer simulations to investigate the impact of housing shape on pressure drop on the blood side and dialysate side, along with removal efficiency.[120] Using an *L*/*D*

ratio fluctuation range of 1–15, they found that a high *L*/*D* ratio increased the pressure drop on the dialysate side, enhancing the uniformity of dialysate flow. Notably, C_L increased with the increase in *L*/*D* ratio. Kosaku *et al.* investigated the impact of housing shape on albumin filtration performance in the *L*/*D* ratio range of 2.9 to 9.3; they found that *L*/*D* ratio adjustments effectively controlled the albumin filtration rate without modifying membrane filtration performance.[90] Furthermore, Donato *et al.* used a two-dimensional mathematical model of solute transport momentum and mass in dialyzers to investigate the impacts of device geometry design, solute transfer processes, and operational parameters on solute removal efficiency.[121] The C_L values of urea, inorganic phosphate, and β_2-MG were consistent with experimental test results. Overall, enhancements of *L*/*D* ratio or *PD* could maximize the ultrafiltration coefficient, thereby guiding improvements in device design.

5 Conclusion

As a core of extracorporeal blood circulation, the CRRT filter has a key role in treatment outcomes; its effectiveness and safety profile are determined by the membrane and the housing design. Many researchers are exploring new membrane materials or modifying existing materials. Membrane filmization, pore structure adjustment, filtration performance improvement, and filter miniaturization can reduce extracorporeal blood volume; functional modifications to the membrane surface can improve biocompatibility and extend filter life, thereby meeting the needs of CRRT. As the requirements for CRRT filters in clinical treatment become increasingly refined, researchers are more carefully considering the impacts of housing design on device effectiveness and safety profile. Investigations of operating mechanisms, particularly regarding mass transfer, have attracted substantial interest. However, research concerning CRRT filter design has been insufficient; in particular, there is no comprehensive system to evaluate the impacts of design factors on device effectiveness and safety profile, nor has there been an in-depth exploration of the effects of various design factors on mass transfer mechanisms. As composite design factors, the *PD* and *L*/*D* ratio have a decisive impact on the device structure and performance. A series of explorations were conducted regarding the mass transfer mechanism, with a focus on the

relationships of *PD* and *L*/*D* ratio with device effectiveness and safety profile, to resolve limitations in CRRT filter design research and seek insights to guide the future design and development of CRRT filters with excellent effectiveness and safety profile.

Chapter 3

Effects of Hollow Fiber Packing Density and Housing Shape on the Solute Removal Performance of CRRT Filters

Chapter 3 Effects of Hollow Fiber Packing Density and Housing Shape on the Solute Removal Performance of CRRT Filters

1 Introduction

CRRT usually removes toxins from the body in a slow and continuous manner, stabilizes hemodynamics, and maintains a homeostatic internal environment. It has positive therapeutic effects in patients with critical illnesses, such as AKI. As core components of CRRT, filters can significantly improve clinical treatment efficacy through minor performance enhancements. Thus far, most filter-related research has focused on dialyzers used in IRRT because they have a longer history compared with CRRT filters. In a previous work, Yamashita *et al*. found that increasing *PD* can improve dialysis performance in IRRT. *PD* values below 30% may reduce the likelihood of dialysate contact with the membrane. Conversely, *PD* values above 50% can strongly enhance internal filtration in a blood system, thereby improving overall solute removal performance in IRRT.[122] Hirano *et al.* reported that housing design had a significant impact on dialyzer dialysis performance.[118] At *PD* values of 48% to 67%, dialyzers with greater *PD* can achieve more robust dialysis performance and enhance the benefit of IRRT. Mineshima *et al*. suggested that increases in *L* and *PD* could increase *TMP*, thereby improving internal filtration and increasing convective transport within a dialyzer.[84, 87] However, dialyzers with *PD* values above 70% had a higher risk of hollow fibers contact, potentially reducing the effective membrane surface area. *PD* values above 70% can also result in hemolysis or membrane leakage through increased pressure loss. Furthermore, Suzuki *et al*. investigated *L*/*D* ratios in the range of 1 to 15; they found that the C_L increased as the *L*/*D* ratio increased, but the C_L was unaffected when the *L*/*D* ratio exceeded 10.[120] Kosaku *et al.* investigated *L*/*D* ratios of 2.9, 5.1, and 9.3; they reported that various *L*/*D* ratios led to significant differences in the performance of filters specifically designed for CRRT using a polyether polymer alloy (PEPA) membrane.[90] However, the lack of systematic research

concerning CRRT filter housing design hinders filter performance enhancement by precluding improvements to housing design.

Housing design optimization based on the same hollow fiber membrane can help to improve membrane performance. In this chapter, the research objective comprised investigating the effect of housing design on the solute removal performances of CRRT filters by evaluating the relationships of *PD* with housing shape (*L*/*D* ratio) and filter performance, which was not conducted by other research groups systematically before. Based on the previous studies and the hollow fibers specifications established in this study, we prepared nine CRRT filters with various combinations of *PD* (50%, 55%, and 60%) and *L*/*D* ratio (2.9, 5.3, and 9.3), then simulated in vitro CVVHD and post-dilution CVVHDF treatment modes. The C_L of each filter was measured using representative LM and MM biomarkers; Doppler ultrasonography was used to detect the $Q_{IF\text{-}Max}$ of each filter. Comparisons of C_L and $Q_{IF\text{-}Max}$ were conducted to determine the optimal combination of design factors for *PD* and *L*/*D* ratio; the results demonstrated the impact of housing design on the solute removal performances of CRRT filters.

2 Materials and Methods

2.1 CRRT Filter Design

Nine CRRT filters with various combinations of *PD* and *L*/*D* ratio were prepared using identical polysulfone (PSf) hollow fiber membranes with *d* and *Δx* of 0.20 mm and 0.04 mm, respectively (Table 3). The k_{UF} of the PSf hollow fiber membrane was 22-23 mL/hr/mmHg, mean pore size was 5-6 nm. The design factors (i.e., *PD* and *L*/*D* ratio) were set to three respective specifications: *PD* = 50% (group 1), *PD* = 55% (group 2), and *PD* = 60% (group 3); *L*/*D* ratio = 2.9 (short and thick (ST)), *L*/*D* ratio = 5.3 (medium (M)), and *L*/*D* ratio = 9.3 (long and slim (LS)). Each group contained filters with the above three *L*/*D* ratios (Table 3). The *PD* and A_o, arithmetic surface area, were calculated by equations (27) and (10), respectively.

$$PD = \left(\frac{d+2\Delta x}{D}\right)^2 N \quad (27)$$

$$A_o = \pi d L N \quad (10)$$

Table 3. Design specifications of CRRT filters.

Group	CRRT filter	*PD* [%]	*L*/*D* ratio [-]	*L* [mm]	*D* [mm]	*N* [-]	A_o [m^2]
1	ST-1	50	2.9	120	41.0	10,710	0.81
	M-1		5.3	180	34.0	7366	0.83
	LS-1		9.3	255	27.4	4788	0.77
2	ST-2	55	2.9	116	40.0	11,264	0.82
	M-2		5.3	175	33.0	7680	0.84
	LS-2		9.3	250	27.0	5120	0.80
3	ST-3	60	2.9	112	38.3	11,264	0.79
	M-3		5.3	166	31.6	7680	0.80
	LS-3		9.3	240	25.8	5120	0.77

CRRT, continuous renal replacement therapy; ST, short and thick; M, medium; LS, long and slim; *PD*, hollow fiber packing density; *L*, effective length of the hollow fiber; *D*, inner diameter of the housing; *N*, number of hollow fibers; A_o, nominal membrane surface area.

2.2 Measurement of Solute Removal Performance

Figure 16(a) shows a schematic of the solute clearance measurement system. Biomarkers of LM comprised urea, creatinine (Cr), and inorganic phosphate (P); a biomarker of MM comprised vitamin B_{12} (VB_{12}). The C_L values of the nine filters for these four biomarkers were measured using two in vitro treatment modes: CVVHD and post-dilution CVVHDF. The initial concentrations of urea, Cr, P, and VB_{12} were 25 mmol/L, 884 μmol/L, 2 mmol/L, and 30 μmol/L, respectively.[80] Pure water was used as the dialysate. In CVVHD mode, the flow rate of the test solution at the blood inlet was 100 mL/min; dialysate entered the dialysate inlet counter currently at a flow rate of 16.7 mL/min (= 1000 mL/hr). In post-dilution CVVHDF mode, the flow rate of the test solution at the blood inlet was also 100 mL/min; dialysate entered the dialysate inlet at a flow rate of 8.3 mL/min and exited the dialysate outlet at a flow rate of 16.7 mL/min. In each mode, the system was operated for 10 minutes; samples were then collected from the inlet and outlet of the experimental filters; and their absorbances were tested with an ultraviolet-visible spectrophotometer (UV-2600; Shimadzu Corporation, Kyoto, Japan). The detection wavelengths of urea, Cr, P, and VB_{12} were 430 nm, 510 nm, 420 nm, 361 nm, respectively. The C_L defined in equation (3) was used as an indicator of solute removal performance. Nine different CRRT filters

were tested three times in each mode to reduce experimental error. All results were expressed as means ± standard deviations. Statistical analyses were performed using unpaired t-tests, and the statistical significance threshold was set to $P < 0.05$.

$$C_{\mathrm{L}} = \left(\frac{C_{\mathrm{BI}} - C_{\mathrm{BO}}}{C_{\mathrm{BI}}}\right) Q_{\mathrm{BI}} + \frac{C_{\mathrm{BO}}}{C_{\mathrm{BI}}} Q_{\mathrm{F}} \quad (3)$$

The C_{L} is an objective index of mass transfer from a medical perspective because it represents the volume of blood from which solutes have been removed. The following parameters are also important from an engineering perspective; they were considered in this study because they are useful in the design of blood purification devices, including $K_{\mathrm{o}}A$, which represents the maximum theoretical clearance of a specific type of the dialyzer for a specific solute when the blood and dialysate flow is infinite, can be obtained from equation (9). N_{T} represents the number of mass transfer unit (equation (11)); larger N_{T} values indicate higher mass transfer efficiency per unit flow rate. Z is the ratio of blood flow to dialysate flow (equation (12)), and E constitutes the maximum solute removal fraction that can be achieved by the dialyzer (equation (13)).

$$K_{\mathrm{o}}A = \frac{Q_{\mathrm{B}}}{\frac{1 - Q_{\mathrm{B}}}{Q_{\mathrm{D}}}} \ln\left(\frac{1 - \frac{C_{\mathrm{L}}}{Q_{\mathrm{D}}}}{1 - \frac{C_{\mathrm{L}}}{Q_{\mathrm{B}}}}\right) \quad (9)$$

$$N_{\mathrm{T}} = \frac{K_{\mathrm{o}}A}{Q_{\mathrm{B}}} \quad (11)$$

$$z = \frac{Q_{\mathrm{B}}}{Q_{\mathrm{D}}} \quad (12)$$

$$E = \frac{C_{\mathrm{L}}}{Q_{\mathrm{B}}} = \frac{1 - \exp[N_{\mathrm{T}}(1 - z)]}{z - \exp[N_{\mathrm{T}}(1 - z)]} \quad (13)$$

2.3 Measurement of Internal Filtration Flow Rate

Figure 16(b) shows a schematic of the internal filtration flow rate measurement system. Whole bovine blood (1 L, 37℃, adjusted to 32% hematocrit) was used on the blood side, and saline was used as the dialysate. The flow setting conditions for the in vitro simulated CVVHD mode were identical to the conditions used for C_{L} measurements. After 15 minutes of operation, Doppler ultrasonography (HI VISION Avius; Hitachi Aloka Medical, Tokyo, Japan) with a pulse-wave value of 7.5 MHz was utilized to measure blood velocity at intervals of 1–2 cm along the direction of blood flow from the blood inlet. The following operating conditions were used:

sampling depth, 1 cm from the outer surface of the housing; sampling gate width, 1.5 cm; and beam angle, 65 °(Figure 17). $Q_{\text{IF-Max}}$ was calculated using equations (14) and (15).

$$S = \frac{1}{4} N\pi L^2 \quad (14)$$

$$Q_{\text{IF-Max}} = Q_{\text{BI}} - Q_{\text{BM}} = V_{\text{BI}}S - V_{\text{BM}}S \quad (15)$$

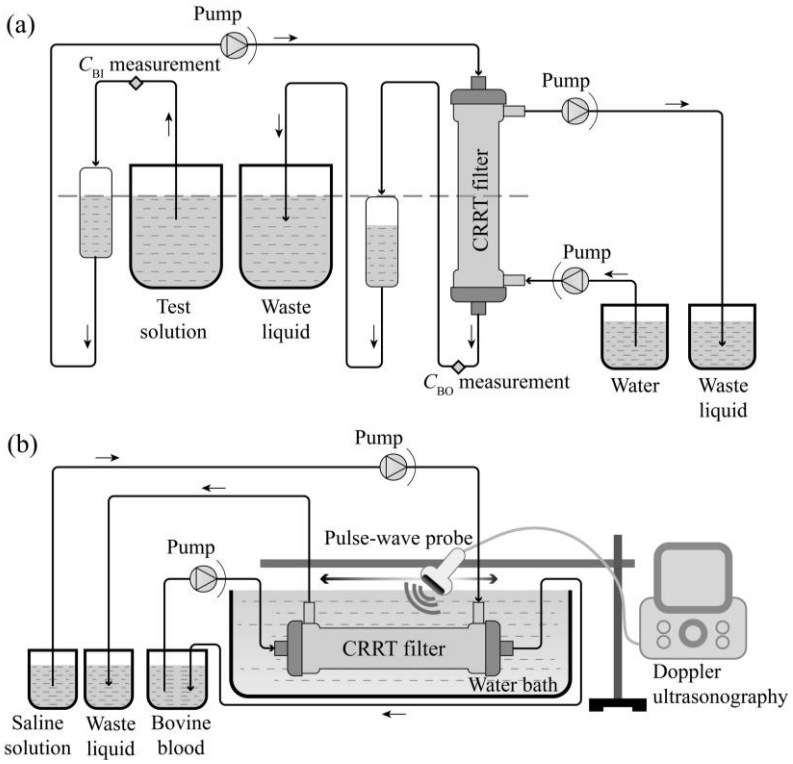

Figure 16. Experimental systems for clearance measurement (a) and internal filtration flow rate measurement (b). C_{BI} and C_{BO} are sample concentrations at the blood inlet and outlet of the blood stream, respectively.

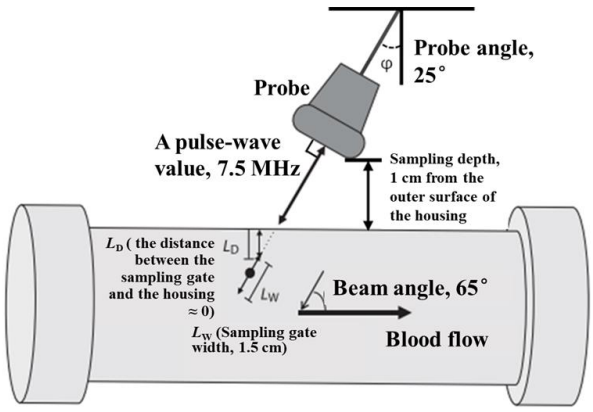

Figure 17. A schematic of Doppler ultrasonography.

3 Results and Discussion

3.1 Optimal CRRT Filter Design

(1) Effect of *L*/*D* Ratio on Solute Removal Performance with Constant *PD*

The C_L values for CRRT filter groups 1 (*PD* = 50%), 2 (*PD* = 55%), and 3 (*PD* = 60%) in CVVHD mode and post-dilution CVVHDF mode are shown in Figure 18. In each mode, the *P* values of clearance for LMs were > 0.05, indicating that the differences were not statistically significant. The C_L for VB_{12} tended to increase as the *L*/*D* ratio increased with constant *PD*. In particular, the C_L for VB_{12} was significantly higher with the LS model than with the ST or the M model (all $P < 0.05$).

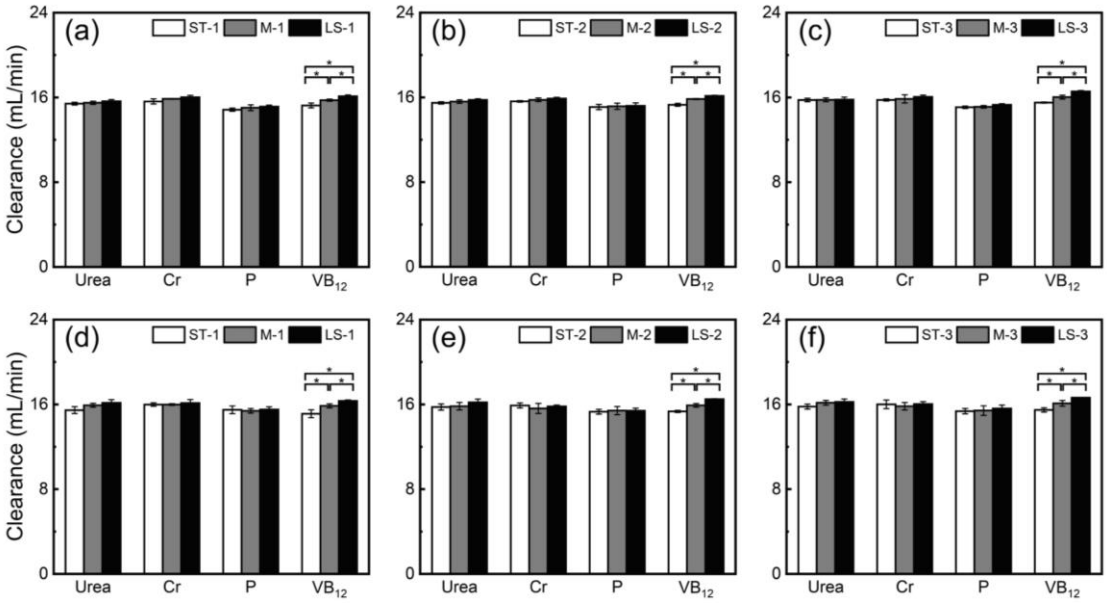

Figure 18. Clearance of continuous renal replacement therapy (CRRT) filter groups 1, 2, and 3 in continuous veno-venous hemodialysis (CVVHD) mode and post-dilution continuous veno-venous hemodiafiltration (post-dilution CVVHDF) mode, $*P < 0.05$. (a) CRRT filter group 1 in CVVHD mode; (b) CRRT filter group 2 in CVVHD mode; (c) CRRT filter group 3 in CVVHD mode; (d) CRRT filter group 1 in post-dilution CVVHDF mode; (e) CRRT filter group 2 in post-dilution CVVHDF mode; (f) CRRT filter group 3 in post-dilution CVVHDF mode. ST, short and thick; M, medium; LS, long and slim.

(2) Effect of *PD* on Solute Removal Performance with Constant *L*/*D* Ratio

The C_L values of the LS series in CVVHD mode are shown in Figure 19. In this mode, the clearance for VB_{12} was higher with the LS-3 model than with the LS-1 or LS-2 model (all $P < 0.05$). The same trend was observed in post-dilution CVVHD mode.

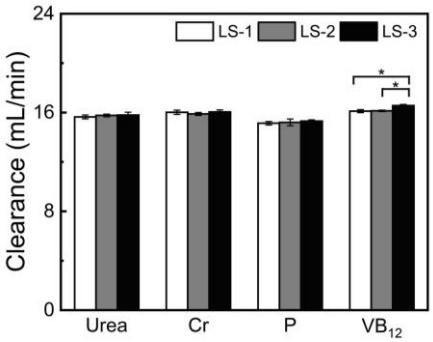

Figure 19. Clearance of LS series in continuous veno-venous hemodialysis (CVVHD) mode, *$P < 0.05$. LS, long and slim.

In both modes, clearances for urea, Cr, and P were not significantly affected by *PD* or *L*/*D* ratio. This lack of effect was recorded because membrane permeability mainly affects the diffusion phenomenon, which influences removal of LMs. In contrast, the effect of design factors is not statistically significant. On the basis of the C_L for VB_{12}, it is clear that C_L values were highest with the LS series; in particular, the C_L of LS-3 was optimal. This phenomenon was observed because the increase in *PD* and *L*/*D* ratio during dialysis increased the pressure drop on the blood side and the dialysate side; the crossflow of blood and dialysate created a larger *TMP* differential that resulted in fluid passage through the membrane, thereby affecting the C_L for VB_{12}.

Based on data of regarding the C_L for VB_{12} in Table 4, the K_oA of the LS-3 was 92.2 mL/min, twofold greater than the K_oA of the ST-1. Therefore, this result demonstrated that better housing design enables better performance from the same membrane. Additionally, the *E* of the LS-3 was 0.166, indicating that the maximum solute removal fraction per unit time was 16.6% (i.e., solute removal through the LS-3 filter was 16.6% of the total solute volume). These data showed that among the nine designs, the LS-3 (*PD* = 60% and *L*/*D* ratio = 9.3) design had the greatest MM removal ability; this housing design was optimal.

Table 4. The K_oA and E of each CRRT filter.

Group	CRRT filter	K_oA [mL/min]	N_T [-]	E [-]
1	ST-1	45.5	0.46	0.152
	M-1	53.8	0.54	0.157
	LS-1	63.5	0.64	0.161
2	ST-2	46.4	0.46	0.153
	M-2	56.2	0.56	0.158
	LS-2	64.5	0.65	0.161
3	ST-3	49.6	0.50	0.155
	M-3	61.0	0.61	0.160
	LS-3	92.2	0.92	0.166

CRRT, continuous renal replacement therapy; K_oA, overall mass transfer-area coefficient; N_T, number of mass transfer units; E, solute removal efficiency; ST, short and thick; M, medium; LS, long and slim.

3.2 Enhancement of Mass Transfer by Internal Filtration

Toxin removal is essential for critically ill patients; however, MMs, especially those with higher molecular weight, lead to greater removal difficulty, compared with LMs. The blood and dialysate flowed in opposite direction in CRRT filter, internal filtration occurs and becomes a driving force for transmembrane mass transfer, which helps to increase the filter's convective removal performance, particularly for MMs. The amount of Q_{IF} indicates the strength of the driving force for transmembrane water movement. The pressure drops on the blood side and the dialysis side have important effects on Q_{IF}. The flow distribution along the direction of blood flow among nine CRRT filters with different *PD*s and *L*/*D* ratios were investigated by Doppler Ultrasonography; then the resultant $Q_{IF\text{-}Max}$ and the aforementioned C_L for VB_{12} were compared to determine which filter design displayed the best dialysis performance.

To accurately explore the effects of *PD* and *L*/*D* ratio on internal filtration, first explored the $Q_{IF\text{-}Max}$ under three different *L*/*D* ratio conditions with constant *PD*. Figure 20(a) clearly shows that the LS-3 with the largest *L*/*D* ratio had the highest $Q_{IF\text{-}Max}$. The $Q_{IF\text{-}Max}$ of LS-3 was 24

mL/min, this value was 76.3% higher than the $Q_{IF\text{-}Max}$ of ST-3 (5.7 mL/min). In this experiment, a larger *L*/*D* ratio indicates that the filter has a longer length and a smaller inner diameter. Under the same blood flow, a larger *L*/*D* ratio was associated with greater pressure drop on the blood side. When the *L*/*D* ratio was largest (*L*/*D* ratio = 9.3), the internal filtration flow rate was highest; moreover, $Q_{IF\text{-}Max}$ = 24 mL/min under Q_B = 100 mL/min is remarkably high, which should significantly contribute to the rate of mass transfer even for MMs with higher *MW*.

Next, we compared the $Q_{IF\text{-}Max}$ under three different *PD*s with constant *L*/*D* ratio. Figure 20(b) shows that the largest *PD* (*PD* = 60%) was associated with the highest $Q_{IF\text{-}Max}$. The $Q_{IF\text{-}Max}$ of LS-3 was 41.7% higher than the $Q_{IF\text{-}Max}$ of LS-1 (14.0 mL/min). This result occurred because, for the same housing size, a larger *PD* resulted in a smaller fluid flow space for the same dialysate flow rate, thereby increasing the pressure drop on the dialysate side and ultimately affecting Q_{IF}. This article omits the $Q_{IF\text{-}Max}$ results of four filters (ST-1, ST-2, M-1, M-2) because, according to the above analysis of design factors, the values of those four filters are smaller than the values of the other five filters. Experimental analysis showed that the increases in design factors (i.e., *PD* and *L*/*D* ratio) effectively enhanced Q_{IF}, agitated convective effects during CRRT treatment, thereby promoting MM removal and improving the performance of CRRT filters.

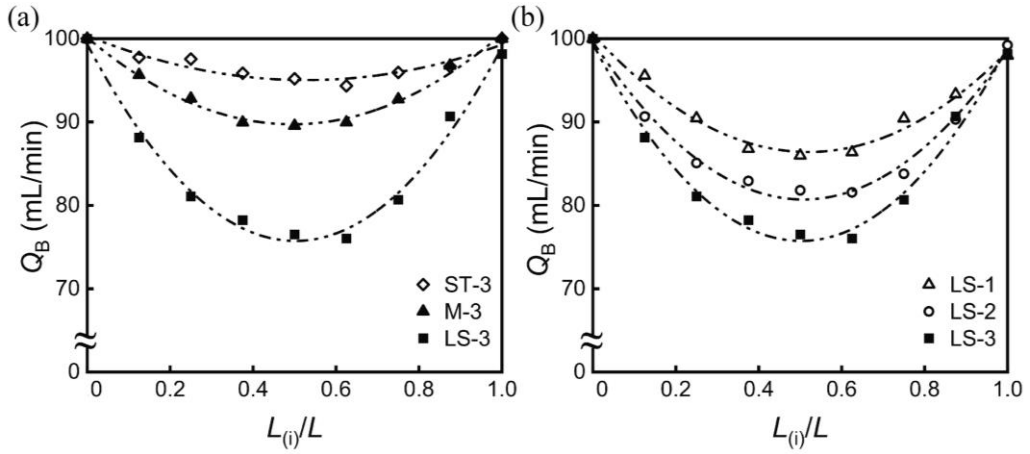

Figure 20. Blood flow rate profiles along the length of the continuous renal replacement therapy (CRRT) filters. (a) hollow fiber packing density (*PD*) = 60%; (b) effective hollow fiber length (*L*) and inner jacket diameter (*D*) ratio (*L*/*D* ratio) = 9.3. ST, short and thick; M, medium; LS, long and slim. $L_{(i)}$ is the position where linear velocity was measured along the CRRT filter.

4 Conclusion

In this chapter, the effects of *PD* and housing shape (*L*/*D* ratio) on solute removal performance were evaluated in CVVHD mode and post-dilution CVVHDF mode. Experimental data showed that the C_L of LMs was not significantly affected by *PD* or *L*/*D* ratio in either mode. However, the C_L of MMs was affected by both *PD* and *L*/*D* ratio in both filtration modes. Furthermore, among the nine test models, the C_L for MMs was optimal when *PD* = 60% and *L*/*D* ratio = 9.3, indicating that the MM removal performance of CRRT filters was affected by housing design specifications. Optimization of the housing design based on the same hollow fiber membrane can maximize membrane performance, which is beneficial for the development of high-performance CRRT filters.

Chapter 4

Effects of Hollow Fiber Packing Density and Housing Shape on the Albumin Filtration Performance of CRRT Filters

Chapter 4 Effects of Hollow Fiber Packing Density and Housing Shape on the Albumin Filtration Performance of CRRT Filters

1 Introduction

CRRT mode diversification and machine design advancements have contributed to the progress of CRRT applications in critical care medicine. As a key determinant of therapeutic efficacy, CRRT filters have more stringent clinical requirements in terms of solute removal performance and safety profile. The effectiveness is mainly determined by the clearances for LMs (e.g., urea, Cr) and MMs (e.g., VB_{12}, MB).[123-124] The previous chapter explored potential relationships between CRRT filter design factors and solute removal performance. Regarding the safety profile, because of the nature of CRRT, patients should be in the most stable state possible. Sudden changes in osmotic pressure because of rapid decreases in water and solute contents, which would exacerbate hemodynamic instability, need to be avoided by maintaining *TMP* stability. Additionally, because the treatment is administered for an extended duration, the leakage of nutrients (e.g., albumin) should be minimized to ensure that the patient can maintain homeostasis.[97, 125] After systematic review and analysis of previous studies, no in-depth studies have been conducted regarding design factors for the aforementioned safety profiles, and no comprehensive evaluation system had been established.

To further characterize the effects of design factors on the safety profile, the effects of *PD* and *L*/*D* ratio on hemodynamic stability and albumin filtration performance were investigated through analyses of nine CRRT filters with various combinations of *PD* and *L*/*D* ratio. The mechanism of protein filtration performance over time was analyzed, and the effects of design factors on the safety profile of CRRT filters were systematically examined through a comprehensive in vitro evaluation system that involved continuous *TMP* monitoring, attenuation of hydraulic permeability, R_C, temporal change in *SC* of albumin, and M_{fld}.

2 Materials and Methods

2.1 CRRT Filter Design

Nine CRRT filters with various combinations of *PD* and *L*/*D* ratio were prepared using identical PSf hollow fiber membranes (Table 3).

2.2 Continuous Transmembrane Pressure and Ultrafiltration Coefficient Monitoring

A schematic diagram of the continuous *TMP* monitoring experiment is shown in Figure 21(a). Two liters of albumin solution (36.0 g/L) were prepared using phosphate-buffered saline with pH = 7.2–7.4. All experiments were performed at 310 K, over a duration of 4 hours, and under conditions of inlet blood flow Q_{BI} = 100 mL/min and Q_F = 10 mL/min. A continuous pressure monitoring system was used to record the P_{BI}, P_{BO}, and P_F at a sampling rate of 1000 times per second. Pressure was averaged over the middle 6 seconds (6000 points) within 10 seconds of data (10,000 points); pressure data were collected at 10-minute intervals from the start of the experiment. *TMP* was calculated as shown in equation (20). The ultrafiltration coefficient, k_{UF}, represents the water permeability of the filter and was calculated as shown in equation (21).

$$TMP = \frac{P_{BI}+P_{BO}}{2} - P_F \quad (20)$$

$$k_{UF} = \frac{Q_{UF}}{TMP} \quad (21)$$

2.3 Concentration Polarization Mass Transfer Resistance Measurement

In the first phase of this experiment, which used experimental conditions identical to the continuous *TMP* monitoring experiment, the P_{BI}, P_{BO}, and P_F at 4 hours were recorded to calculate TMP_1. In the second phase of this experiment, phosphate-buffered saline was connected to the blood inlet. After the filter had been washed for 5 minutes, the P_{BI}, P_{BO}, and P_F were recorded; this

analysis allowed calculation of TMP_2 while minimizing the effect of concentration polarization. In this experiment, R_t included R_m, R_c, and R_f, as shown in equation (22).

$$R_t = R_f + R_m + R_c \quad (22)$$

R_t was calculated through the division of TMP_1 by J and μ (equation (23)).[93]

$$R_t = \frac{TMP_1}{J \cdot \mu} \quad (23)$$

$R_f + R_m$ was obtained from TMP_2.

$$R_f + R_m = \frac{TMP_2}{J \cdot \mu} \quad (24)$$

R_c was calculated as shown in equations (22-24).

2.4 Variation in Albumin Sieving Coefficient Over Time and Measurement of Albumin Removal

A schematic diagram of the sieving coefficient experiment is shown in Figure 21(b). Under experimental conditions identical to the continuous *TMP* monitoring experiment, the analysis of *SC* was performed with 2 L of albumin solution (36.0 g/L) for 4 hours. Samples were collected at 10-minute intervals at the blood inlet/outlet and filtrate outlet to measure albumin concentrations. *SC* and M_{fld} were calculated as shown in equations (25) and (26), respectively.

$$SC = \frac{2C_F}{C_{BI} + C_{BO}} \quad (25)$$

$$M_{fld} = \int_0^t Q_F \, C_F dt \quad (26)$$

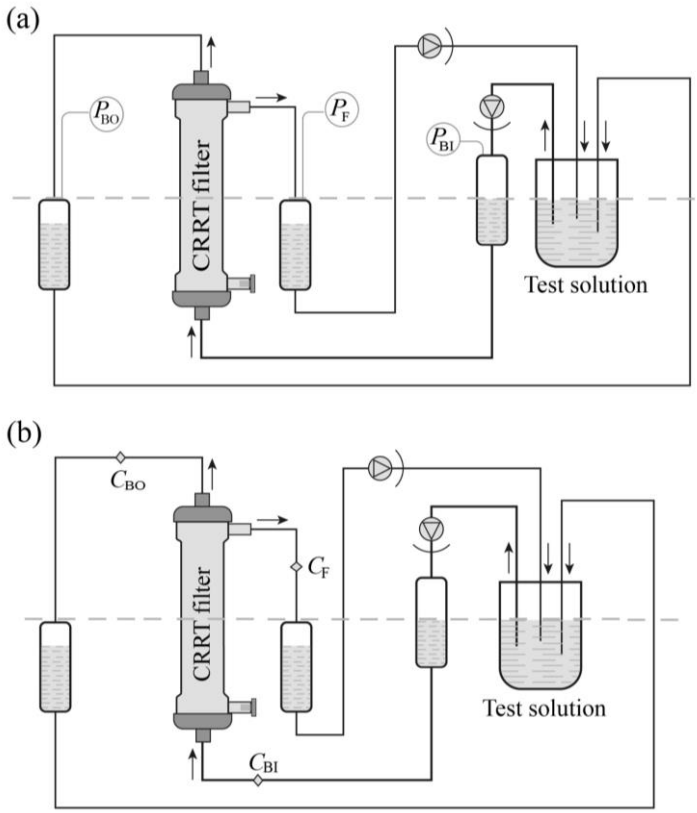

Figure 21. Schematic diagrams of continuous transmembrane pressure (*TMP*) monitoring (a) and sieving coefficient (*SC*) experiments (b). P_{BI}, blood inlet pressure; P_{BO}, blood outlet pressure; P_F, filtrate pressure; C_{BI}, C_{BO}, and C_F, concentrations at the blood inlet/outlet and filtrate outlet, respectively.

3 Results and Discussion

3.1 Effects of Design Factors on Transmembrane Pressure and Ultrafiltration Coefficient

The *TMP* directly influences CRRT filter effectiveness and safety profile. Conventional pressure monitoring methods obtain *TMP* data by recording the blood outlet pressure and dialysate outlet pressure, then calculating the difference between these values as a *TMP*. The monitoring frequency is 5–100 seconds per recording, which hinders accurate and continuous monitoring of *TMP*. Here, we used a pressure monitor with high-frequency sampling (1000 times/second) to conduct real-time measurements of P_{BI}, P_{BO}, and P_F. Even when blood flow and dialysate flow

were both low, small changes in *TMP* were observed, and the accuracy of pressure monitoring was considerably improved. These advances facilitated exploration of the effects of *TMP* on filter effectiveness and safety profile.

The trends of variation in *TMP* are shown in Figure 22(a, b). The *TMP* of each CRRT filter initially tended to increase rapidly, then gradually increased over time. The range of variation was 2 mmHg, which indicated high stability and suggested that design factors did not extensively influence filter hemodynamic stability in the ranges of *PD* and *L*/*D* ratio explored in this study. Additionally, in terms of assessing effectiveness, k_{UF} is inversely proportional to *TMP* (i.e., *TMP* increases and k_{UF} decreases); thus, when Q_F is constant, an increase in *TMP* leads to a decrease in the water permeability of the filter. The trends of attenuation in k_{UF} over time are shown in Figure 22(c, d), where $k_{UF}(0)$ represents the initial detection value of k_{UF}. Values of k_{UF} of the nine filters were attenuated within 60 minutes of the beginning of the experiment; the attenuation within 4 hours was < 10%. Although the formation of a protein cake layer resulted in a gradual decline in water permeability, each filter was able to maintain stable effectiveness within the ranges of *PD* and *L*/*D* ratio explored in this study.

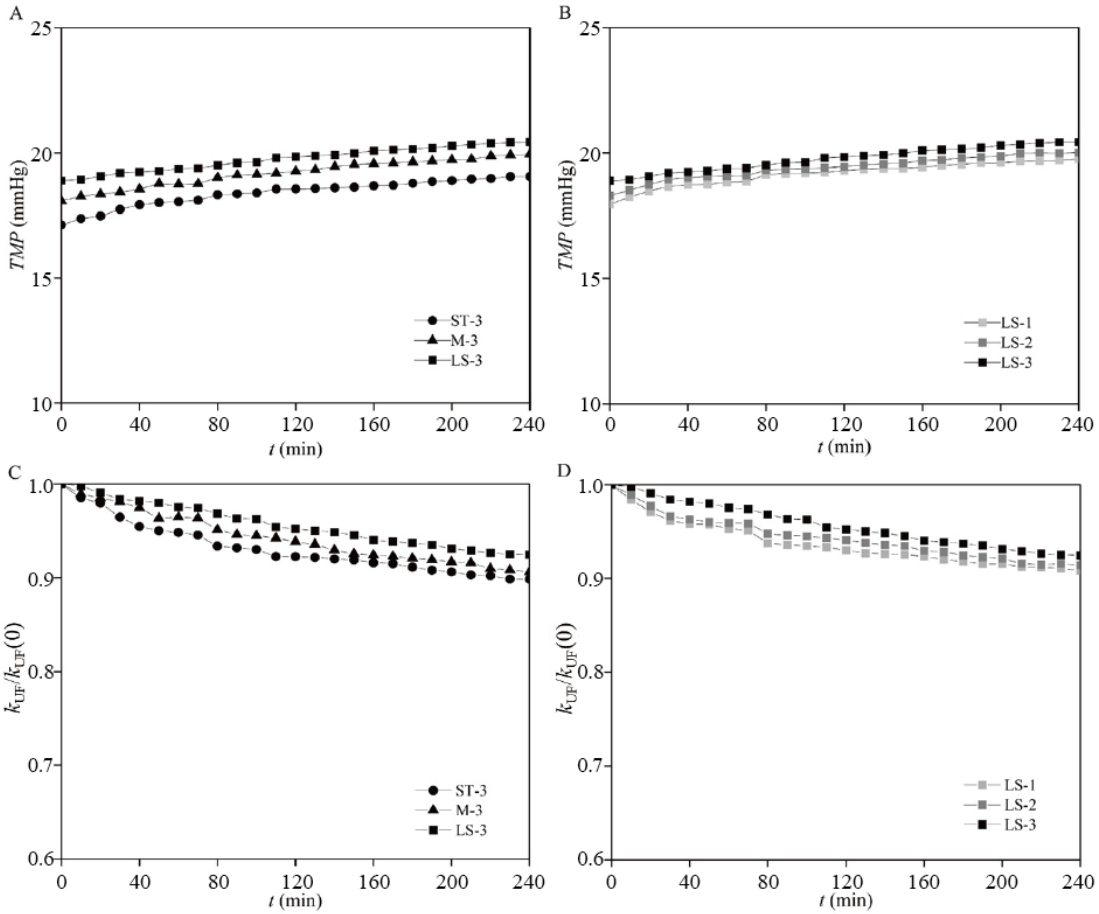

Figure 22. Trends of variation in transmembrane pressure (*TMP*) and the ultrafiltration coefficient (k_{UF}). *TMP*, (a), hollow fiber packing density (*PD*) = 60%; (b), effective hollow fiber length (*L*) and inner housing diameter (*D*) ratio (*L*/*D* ratio) = 9.3; k_{UF}, (c), *PD* = 60%; (d), *L*/*D* ratio = 9.3. ST, short and thick; M, medium; LS, long and slim.

3.2 Effects of Design Factors on Concentration Polarization

Concentration polarization, an important indicator of protein filtration performance, refers to a phenomenon that occurs during membrane filtration. Specifically, the protein concentration is higher in the concentration polarization layer than in the bulk solution; moreover, the extent of protein filtration is enhanced in the concentration polarization layer. Importantly, reduced formation of a concentration polarization layer leads to less albumin filtration. R_c is used to quantitatively evaluate the concentration polarization layer on the membrane surface; an increase in R_c indicates a larger concentration polarization layer. The R_c measurements for each CRRT filter

are shown in Figure 23. When the *PD* was constant, the R_c value decreased as the *L*/*D* ratio increased; the R_c value of LS-3 was significantly lower than the those of ST-3 and M-3 (both $P < 0.05$). Furthermore, when the *L*/*D* ratio was constant, the R_c value decreased as the *PD* increased; the R_c value of LS-3 was significantly lower than those of LS-1 and LS-2 (both $P < 0.05$). The lowest R_c value among the nine CRRT filters was observed with *PD* = 60% and *L*/*D* ratio = 9.3, indicating that the concentration polarization layer of LS-3 was smallest; this finding suggested that design factors have a substantial effect on the formation of a concentration polarization layer in CRRT filters, thereby influencing the extent of protein filtration.

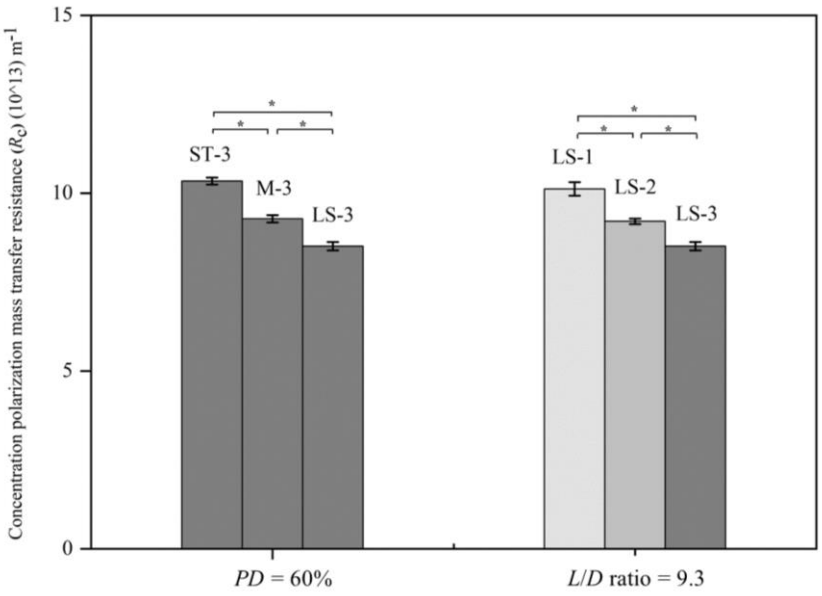

Figure 23. Concentration polarization mass transfer resistance of CRRT filters (*$P < 0.05$). *PD*, hollow fiber packing density; *L*/*D* ratio, effective hollow fiber length (*L*) and inner jacket diameter (*D*) ratio. ST, short and thick; M, medium; LS, long and slim.

3.3 Effects of Design Factors on Albumin Filtration Performance

SC is an important index used to measure the filtration performance of a filter for a specific solute. A larger *SC* value for a target solute indicates stronger filtration performance for that solute. However, the filtration of useful solutes, such as albumin (i.e., non-target solutes), must be suppressed within a particular range. *SC* is limited by the hollow fiber membrane, as well as the

filter design. Temporal trends of variation in the *SC* of albumin are shown in Figure 24. *SC* was maximal at the beginning of the experiment and then decreased over time; specifically, *SC* dramatically declined in the first 20 minutes, then continued to decline at a slower rate. After 60 minutes, *SC* became stabilized at a nearly identical value for all filters. When the *PD* was constant, the *SC* value decreased with increases in the *L*/*D* ratio, as follows: $SC_{ST\text{-}3} > SC_{M\text{-}3} > SC_{LS\text{-}3}$ (Figure 24(a)). Moreover, when the *L*/*D* ratio was constant, the *SC* value decreased with increases in the *PD*, as follows: $SC_{LS\text{-}1} > SC_{LS\text{-}2} > SC_{LS\text{-}3}$ (Figure 24(b)). The lowest *SC* value among the nine CRRT filters was observed with *PD* = 60% and *L*/*D* ratio = 9.3. This filter exhibited the least albumin filtration, presumably because design factors affected the formation and development of the concentration polarization layer, leading to reduced albumin filtration.

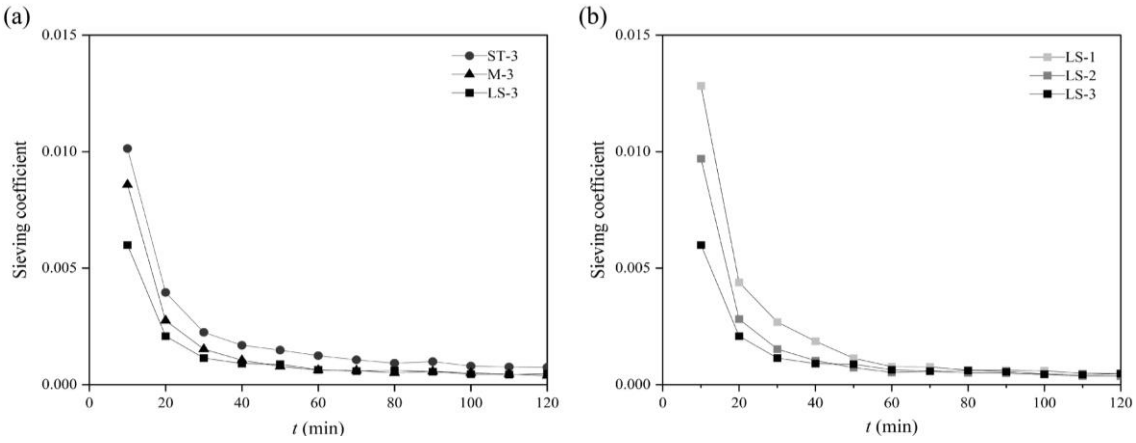

Figure 24. Trends of variation in albumin sieving coefficient. (a), hollow fiber packing density (*PD*) = 60%; (b), effective hollow fiber length (*L*) and inner jacket diameter (*D*) ratio (*L*/*D* ratio) = 9.3. ST, short and thick; M, medium; LS, long and slim.

Albumin is the most abundant protein in plasma; it plays a prominent role in maintaining stable plasma colloid osmotic pressure. The primary goal of CRRT is maintenance of the patient's hemodynamic stability and reduction of nutrient loss. Therefore, the filter design should minimize the extent of albumin filtration (also known as "albumin loss" or "albumin leakage", usually not called as "albumin removal" in clinical situation but in scientific discussion as follows) and improve the overall safety profile. The amounts of albumin removed within 4 hours are shown in Figure 25. Increases in *PD* and *L*/*D* ratio led to less albumin filtration ($P < 0.05$). Among the nine

CRRT filters, the smallest M_{fld} was observed with *PD* = 60% and *L*/*D* ratio = 9.3. The extent of albumin filtration was reduced by 47.5% compared with the ST-1 design, which had the maximum M_{fld} (LS-3, 79.92 ± 0.13 mg vs ST-1, 152.27 ± 6.01 mg). These results suggested that the tested design factors can control the extent of protein removal and improve the safety profiles of CRRT filters.

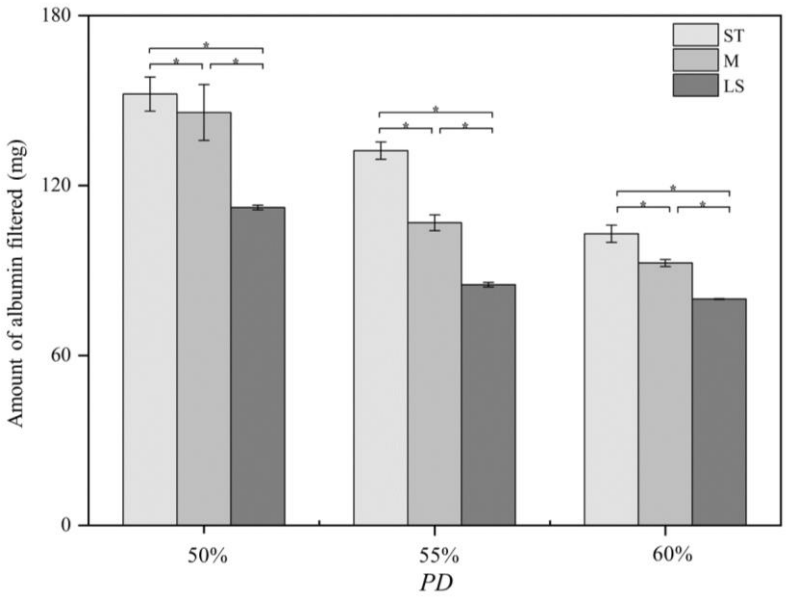

Figure 25. Amount of albumin filtered (*P < 0.05). *PD*, hollow fiber packing density. ST, short and thick; M, medium; LS, long and slim.

4 Conclusion

In this chapter, five in vitro indicators were used to analyze the mechanism of protein filtration performance over time, and a comprehensive in vitro evaluation system was established to explore the effects of various design factors on the safety profile of CRRT filters. Within the range of parameters evaluated in this study, two design factors (i.e., *PD* and *L*/*D* ratio) demonstrated minimal effects on *TMP* variation and k_{UF} attenuation. Nine filters were able to maintain hemodynamic stability and suppress the attenuation of water permeability; the filter with *PD* of 60% and *L*/*D* ratio of 9.3 removed the smallest amount of albumin. These results suggest that an appropriate increase in *PD* and the use of an elongated housing shape can suppress

albumin filtration (albumin loss) and improve the safety profile of CRRT filters. Performance improvements in CRRT filters are essential for further improvements in therapeutic efficacy, which are necessary for the development of CRRT filters that exhibit excellent effectiveness and a robust safety profile.

Chapter 5

A Practical Design Equation for Accurate Quantification of CRRT Filter Design Factors and Convection Effects

Chapter 5 A Practical Design Equation for Accurate Quantification of CRRT Filter Design Factors and Convection Effects

1 Introduction

Because of its ability to removal toxins without affecting hemodynamic stability, CRRT is one of the most preferred treatments for critical care medicine. Technological advancements have led to broad usage of CRRT in the treatment of critical illnesses (e.g., sepsis and multi-organ dysfunction syndrome); its applications have expanded beyond supporting kidney functions. Considering the increasing clinical need for CRRT, further improvement in blood purification therapeutic efficacy has become an important focus for researchers. CRRT is conducted to remove accumulated toxins with different molecular weights from a patient's body, with a particular focus on MMs. Biomarkers of MMs include β_2-MG and MB. The accumulation of β_2-MG can lead to pathological fractures and induce cardiovascular disease[126-128]; MB is the main causative factor of acute myoglobinuric kidney injury[129-130]. CRRT filters have key roles in blood purification therapeutic efficacy; their performances depend on membrane performance and filter design. Regarding filter design, previous studies revealed relationships between design factors and filter performances through mathematical models and experiments, offering a new approach for optimizing filter design; however, those studies primarily focused on LMs (represented by urea).[120-121] The removal efficiency and mechanism of MMs (represented by β_2-MG) have not been fully elucidated. Moreover, no practical design equations have systematically integrated mathematical models and experimental results to accurately and efficiently quantify the design factors that influence CRRT filters and convection effects.

In this chapter, we designed nine CRRT filters with various combinations of *PD* and *L*/*D* ratio to measure the C_L for β_2-MG and MB in an in vitro simulated CVVHD mode. We also used the Doppler ultrasonography to measure $Q_{IF\text{-}Max}$ as an aid; this approach facilitated an exploration

of the impacts of various design factors on convection effects, revealing the mechanisms that influence MM removal performance. Furthermore, we established a multiple linear regression model for statistical analysis of the $Q_{IF\text{-}Max}$. The impacts of design factors on the $Q_{IF\text{-}Max}$ were systematically investigated and experimentally verified. Finally, we proposed a practical design equation to accurately quantify the design factors that influence CRRT filters and convection effects.

2 Materials and Methods

2.1 CRRT Filter Design

Nine CRRT filters with various combinations of *PD* and *L*/*D* ratio were designed using identical PSf hollow fiber membranes (Table 3).

2.2 Measurement of MM Removal Performance

Figure 16(a) shows a schematic of the MM clearance measurement system. The C_L values of nine CRRT filters for β_2-MG and MB were examined using an in vitro simulated CVVHD mode. The initial concentrations of β_2-MG and MB were 1.5 mg/L and 100 mg/L, respectively; saline was used as the dialysate. The test solution flowed into the blood inlet at a flow rate of Q_{BI} = 100 mL/min; the dialysate flowed into the dialysate inlet at a flow rate of Q_D = 16.7 mL/min (= 1000 mL/hr). After the system had operated for 10 minutes, samples were collected at the blood inlet and outlet. Sample concentrations of β_2-MG were tested using a biochemical analyzer (Thermo Konelab 20; Thermo Fisher Scientific Inc., Waltham, MA, USA). Sample concentrations of MB were tested using a UV-Vis spectrophotometer (UV-2600; Shimadzu Corporation, Kyoto, Japan). The C_L, an important index for evaluation of filter performance, was defined in equation (3). Statistical analyses were performed using unpaired t-tests, and the threshold for *P* was set at < 0.05.

$$C_L = \left(\frac{C_{BI} - C_{BO}}{C_{BI}}\right) Q_B + \frac{C_{BO}}{C_{BI}} Q_F \qquad (3)$$

2.3 Measurement of Internal Filtration Flow Rate

Figure 16(b) shows a schematic of internal filtration flow rate measurement. Whole bovine blood (1 L, 37℃; adjusted to 32% hematocrit) was used on the blood side; saline was used as the dialysate. Flow setting conditions in vitro simulated CVVHD mode were identical to the conditions used for C_L measurements. After 15 minutes of operation, Doppler ultrasonography (HI VISION Avius; Hitachi Aloka Medical, Tokyo, Japan) with a pulse-wave value of 7.5 MHz was used to measure blood velocity at intervals of 1–2 cm along the direction of blood flow from the blood inlet. The following operating conditions were used: sampling depth, 1 cm from the outer surface of the housing; sampling gate width, 1.5 cm; and beam angle, 65 °(Figure 17). $Q_{IF\text{-}Max}$ was calculated using equations (14) and (15).

$$S = \frac{1}{4} N\pi L^2 \tag{14}$$

$$Q_{\mathrm{IF-Max}} = Q_{\mathrm{BI}} - Q_{\mathrm{BM}} = V_{\mathrm{BI}}S - V_{\mathrm{BM}}S \tag{15}$$

2.4 Establishment of a Practical Design Equation to Quantify Design Factors and Convection Effects

Because the same PSf hollow fiber membrane (d = 0.20 mm, Δx = 0.04 mm, k_{UF} = 22-23 mL/hr/mmHg, mean pore size = 5-6 nm) was used in this study, PD was determined by N and D^2 (equation (27)). Statistical Package for the Social Sciences (SPSS, version 28.0.1.0) software was used for statistical analysis of the $Q_{IF\text{-}Max}$; a multiple linear regression model was established with N/D^2 and L/D ratio as explanatory variables to explore the impacts of design factors on $Q_{IF\text{-}Max}$. Statistical analyses of the $Q_{IF\text{-}Max}$ of ST-1, LS-1, LS-2, ST-3, M-3, and LS-3 were performed to obtain a design equation that could quantify design factors and convection effects (equation (28)). The F-test was used to determine model significance; a large F-value indicated that the results of regression analysis were statistically significant.

$$PD = \left(\frac{d+2\Delta x}{D}\right)^2 N \tag{27}$$

$$Q_{\mathrm{IF-Max}} = \mathrm{b}_0 + \mathrm{b}_1\left(\frac{N}{D^2}\right) + \mathrm{b}_2\left(\frac{L}{D}\right) \tag{28}$$

where b_1 and b_2 are the regression coefficients of each variable factor, and b_0 is a constant term.

The above model was standardized as follows:

$$\mathrm{B}(Q_{\mathrm{IF-Max}}) = \beta_1 \mathrm{B}\left(\frac{N}{D^2}\right) + \beta_2 \mathrm{B}\left(\frac{L}{D}\right) \quad (29)$$

where β_1 and β_2 are the standard coefficients of each variable factor.

Based on the standard coefficients, the impact ratio of each explanatory variable relative to $Q_{\mathrm{IF\text{-}Max}}$ was expressed as follows:

$$\text{Impact ratio} = \frac{\beta_i^2}{\sum_{i=1}^{2} \beta_i^2} \times 100\% \quad (30)$$

A larger impact ratio of the variable factor indicates that it has a stronger impact on $Q_{\mathrm{IF\text{-}Max}}$.[131] To evaluate the generalizability of equation (28), we randomly selected M-1, ST-2, and M-2, then inserted their design factor parameters into the design equation; the results were compared with measurements by the Doppler ultrasonography to identify statistically significant differences.

3 Results and Discussion

3.1 Effects of Design Factors on MM Removal Performance and Internal Filtration Flow Rate

The C_L measurements of β_2-MG and MB in each CRRT filter within the CVVHD mode are shown in Figure 26(a, b). When the *L*/*D* ratio was constant (*L*/*D* ratio = 9.3), the C_L values for β_2-MG and MB increased as the *PD* increased; however, there were no statistically significant differences among LS-3, LS-1, and LS-2, indicating that the *PD* had minimal impact on C_L (Figure 26(a)). When the *PD* was constant (*PD* = 60%), the C_L values for both substances increased as the *L*/*D* ratio increased. The C_L values for β_2-MG and MB in LS-3 were 15.5 ± 0.3 mL/min and 13.4 ± 0.1 mL/min, respectively; these significantly differed from the values in M-3 and ST-3 (all $P < 0.05$). Moreover, the C_L values for β_2-MG and MB in LS-3 were 14.2% and 15.7% higher than the corresponding values in ST-3 (β_2-MG, 13.3 ± 0.3 mL/min; MB, 11.3 ± 0.2 mL/min), indicating that LS-3 (*PD* = 60% and *L*/*D* ratio = 9.3) had substantially better MM removal performance (Figure 26(b)).

Variations in blood flow according to the direction of flow among CRRT filters are shown in Figure 26(c, d). When pressure was higher on the blood inlet side than on the dialysate outlet side, forward filtration occurred; the blood flow rate decreased along the direction of blood flow. Conversely, when pressure was higher on the dialysate inlet side than on the blood outlet side, backward filtration occurred; the blood flow rate increased. In the CVVHD mode, when the *L*/*D* ratio was constant (*L*/*D* ratio = 9.3), $Q_{IF\text{-}Max}$ increased as the *PD* increased (Figure 26(c)); when the *PD* was constant (*PD* = 60%), $Q_{IF\text{-}Max}$ increased as the *L*/*D* ratio increased (Figure 26(d)). The $Q_{IF\text{-}Max}$ of LS-3 was highest at 24.7 ± 2.2 mL/min, this value was 38.3% higher than the $Q_{IF\text{-}Max}$ of LS-1 (15.2 ± 1.7 mL/min) and 70.7% higher than the $Q_{IF\text{-}Max}$ of ST-3 (7.2 ± 0.3 mL/min), indicating that the *L*/*D* ratio had a greater impact on the $Q_{IF\text{-}Max}$ than the *PD*.

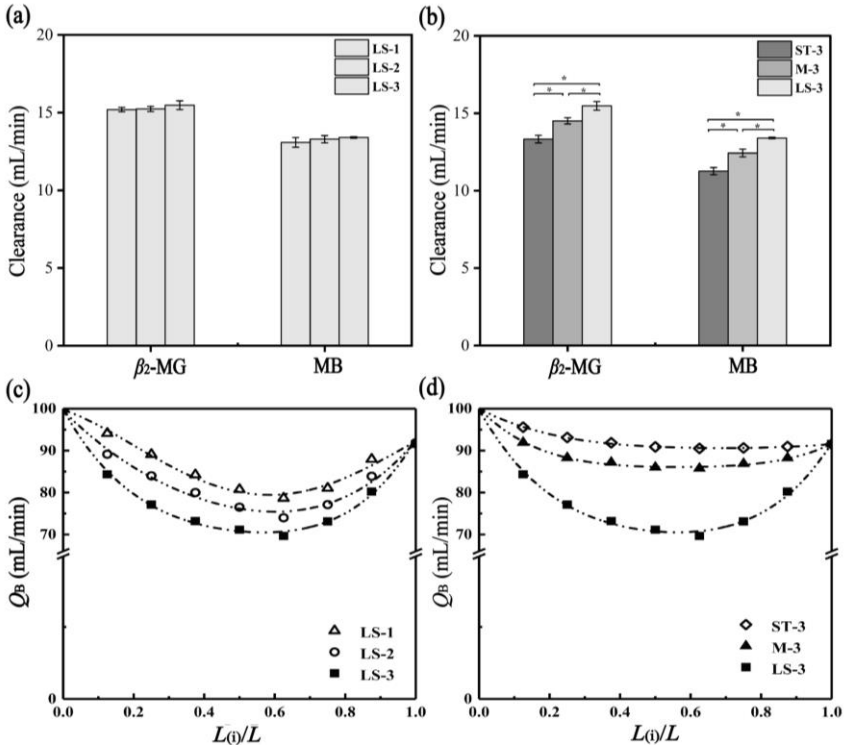

Figure 26. Clearances (C_L) for β_2-MG and MB in continuous veno-venous hemodialysis (CVVHD) treatment mode (a and b, *P < 0.05). Blood flow rate profiles along the direction of blood flow in continuous renal replacement therapy (CRRT) filters (c and d). (a) and (c), *L*/*D* ratio = 9.3 with varying *PD* (50%, 55%, or 60%); (b) and (d), *PD* = 60% with varying *L*/*D* ratio (2.9, 5.3, or 9.3). $L_{(i)}$ is the position where linear velocity was measured along the CRRT filter. ST, short and thick; M, medium; LS, long and slim.

β_2-MG and MB are two representative MMs, although the former is normally a toxic substance but the latter is not; their removal has clinically significant implications for patients with AKI who require renal replacement therapy. We measured the C_L of LMs in chapter 3 and found that the C_L values were close to the blood flow rate under CRRT treatment conditions, which indicated that LMs were mainly removed by diffusion because of their smaller *MW*. Based on the PSf hollow fiber membrane (d = 0.20 mm, Δx = 0.04 mm, k_{UF} = 22-23 mL/hr/mmHg, mean pore size = 5-6 nm) used in this study, the C_L of LMs were close to the maximum regardless of the housing design. C_L measurements revealed that LS-3 had the best VB_{12} removal performance, as shown in Figure 26(a) and (b), which indicated that the design factors had a significant impact on the MMs removal. From engineering point of view, in the filter, there are two driving force for the mass transfer, diffusion and convection effects. The MMs with higher *MW* require increased convection to compensate for insufficient diffusion removal performance. Optimal design factors effectively enhanced convection, thereby promoted MM removal performance of CRRT filters. Here, we used the Doppler ultrasonography to measure the internal filtration flow rates of nine filters in a CVVHD treatment model; subsequently, we quantitatively evaluated the impacts of different design factors on convection effects. The results showed that LS-3 had the highest $Q_{IF\text{-}Max}$ in Figure 26(c) and (d). According to the Hagen–Poiseuille equation[84], respective increases in the *PD* and *L*/*D* ratio reduced dialysate flowable space and elongated the filter, thereby increasing blood–dialysate convection; these changes led to greater pressure drop, thus promoting internal filtration and enhancing convection effects. The internal filtration flow test showed that, compared with the increase in *PD*, the increase in *L*/*D* ratio was more effective in terms of enhancing the convection effect in the filter. The consistent impact of design factors on MM removal performance and internal filtration efficiency demonstrated that the removal of these substances was primarily dependent on convection. Thus, effective quantitative analysis of convection effects could help to predict the MM removal performances of CRRT filters.

3.2 A Practical Design Equation to Quantify Design Factors and Convection Effects

Based on the above results, two variable factors (N/D^2 and L/D ratio) and $Q_{IF\text{-}Max}$ were used to create a multiple linear regression model of design factors and convection effects; this model was utilized to analyze the impact of each variable factor on the convection effects, and an *F*-test was conducted to evaluate model significance. The model's adequacy was evaluated using analysis of variance, as shown in Tables 5 and 6. The *F*-value of 78.871 was above the threshold for $F_{0.05}(2,9)$, and the *P*-value was < 0.05, indicating that the model was plausible. The adjusted R^2 value was 0.934, implying that changes in N/D^2 and L/D ratio could explain 93.4% of the variation in $Q_{IF\text{-}Max}$ (Table 5). The effects of each variable on $Q_{IF\text{-}Max}$ are shown in Table 6. The regression coefficients were b_0 = -34.775 mL/min, b_1 = 4.749 mL·mm^2/min, and b_2 = 2.293 mL/min. In the CVVHD treatment model, the following design equation was established to quantify design factors and convection effects:

$$Q_{\mathrm{IF-Max}} = -34.775 + 4.749 \times \frac{N}{D^2} + 2.293 \times \frac{L}{D} \qquad (31)$$

$Q_{IF\text{-}Max}$ was significantly affected by N/D^2 and L/D ratio (all $P < 0.05$). The standard coefficients of N/D^2 and L/D ratio for $Q_{IF\text{-}Max}$ were β_1 = 0.386 [-] and β_2 = 0.921 [-], respectively. Upon substitution of these values into equation 30, the calculated impacts of N/D^2 and L/D ratio on $Q_{IF\text{-}Max}$ were 15.0% and 85.0%, respectively.

Table 5. Analysis of variance for the multiple linear regression model of design factors and convection effects

CVVHD	Sum of Squares	DF	Mean Square	*F*	*P*	Adjusted R^2
Regression	596.277	2	298.138			
Residual	34.021	9	3.780	78.871	.000	0.934
Total	630.298	11				

Table 6. Effects of standard coefficients and variable factors on $Q_{IF\text{-}Max}$

CVVHD	b	Std. Error	β	*P*
b_0	-34.775 mL/min	7.042	-	0.001
N/D^2	4.749 mL·mm^2/min	0.955	0.386	0.001
L/D	2.293 mL/min	0.193	0.921	0.000

Here, we constructed a practical design equation to analyze convection effects efficiently and accurately quantitatively in CRRT filters through the quantification of design factors and convection effects. Evaluation of the multiple linear regression model through analysis of variance revealed $F > F_{0.05}$, $P < 0.05$, and $R^2 > 0.9$; these findings indicated that the practical design equation had high reliability.[132-134] The design equation showed that, among the factors influencing $Q_{IF\text{-}Max}$, L/D ratio had a much greater impact on convection effects, compared with N/D^2. Therefore, L/D ratio optimization can significantly increase $Q_{IF\text{-}Max}$ and enhance convection effects, thus improving the MM removal performances of CRRT filters. To further explore the generalizability and accuracy of the design equation, $Q_{IF\text{-}Max}$ was calculated by randomly entering design factor parameters of M-1, ST-2, and M-2 into equation (31). $Q_{IF\text{-}Max}$ was also measured using the Doppler ultrasonography. Independent samples *t*-tests were used to validate two sets of data; differences between the calculated values of the design equation and the measured values were statistically evaluated (Table 7). The *P*-value of 0.877 was > 0.05, indicating that there was no statistically significant difference between the calculated and measured values. The design equation for the design factors and convection effects was generalizable within the range of design factor parameters used in this study.

Table 7. Differences between calculated and measured values of the design equation for quantification of design factors and convection effects

CRRT filter	*PD* [%]	N/D^2 [mm^{-2}]	L/D ratio [-]	$Q_{IF\text{-}max}$ [mL/min]		*t*	*P*
				Calculated value	Measured value		
M-1	50%	6.37	5.3	7.64	8.56		
ST-2	55%	7.04	2.9	5.31	5.45	-0.164	0.877
M-2	60%	7.05	5.3	10.87	10.7		

4 Conclusion

In this chapter, our systematic synthesis of mathematical models and experimental results facilitated the establishment of a practical design equation that accurately and efficiently quantifies the design factors of CRRT filters and convection effects. The proposed design equation allows rapid quantification of the $Q_{IF\text{-}Max}$, or convection effects, through simple substitution of design factor parameters without the requirement for filter sample production or experimental investigation. Thus, it effectively predicts the MM removal performances of CRRT filters with different design factors, contributing to more efficient design of new CRRT filters.

Chapter 6

Summary

Chapter 6 Summary

Continuous Renal Replacement Therapy (CRRT) refers to all continuous and slow water and solute removal treatments intended to provide long-term support mainly for renal function in critically ill patients with hemodynamic instability in the ICU. In this study, Chapter 1 provided an overview of the evolution, main treatment modes, and clinical importance of CRRT. Since Kramer *et al.* proposed CAVH in 1977 and implemented it in clinical practice, CRRT has gained broad usage in critical care medicine. This usage has arisen from treatment mode diversification, as well as progress in the design of related consumables and blood purification devices. CRRT has become the recommended treatment approach for acute kidney injury (AKI) because of its capacity to remove multiple uremic toxins while maintaining hemodynamic stability. Advances in technology have facilitated the use of CRRT in the treatment of critical illnesses such as sepsis and multi-organ dysfunction syndrome (MODS); it has expanded from supporting renal function to supporting the functions of organs such as the heart, liver, and lung. Therefore, further improvement in the blood purification treatment effect of CRRT has become a key research focus.

Chapter 2 provided an overview of the main factors and performance indicators that affect CRRT filter performance. CRRT filters are hollow fiber structures developed from dialyzers for conventional hemodialysis therapy. For each filter, the effectiveness and safety profile are determined by the performance of the internal hollow fiber membrane and the external housing design. Thus far, there have been few in vitro studies regarding CRRT filters; most previous studies focused on improvements in membrane performance to satisfy the clinical need for continuous treatment lasting more than 24 hours. There has been minimal in-depth exploration of the effects of various design factors on filter performance. Furthermore, dialyzer performance indicators are frequently used to evaluate CRRT filter performance; there is no comprehensive system for evaluating the effectiveness and safety profile of CRRT filters.

CRRT filter effectiveness is mainly determined by the clearances for LMs (e.g., urea, Cr, and P) and MMs (e.g., VB_{12}, β_2-MG, and MB). In terms of the safety profile, CRRT filters are required to maintain maximum *TMP* stability during long-term treatment; this avoids the exacerbation of hemodynamic instability because of rapid changes in water and solute concentrations.

Furthermore, it is possible to minimize the cumulative loss of nutrients (e.g., albumin) while maintaining overall homeostasis.

Chapters 3–5 presented a series of studies that evaluated the relationships of design factors with the effectiveness and safety profile of CRRT filters by analyzing nine different combinations of *PD* and housing shape (*L*/*D* ratio). Relationships between design factors and CRRT filter removal performance were explored in Chapter 3. We were the first to conduct Doppler ultrasonography to measure the $Q_{\text{IF-Max}}$ of CRRT filters and then facilitated an exploration of the effects of various design factors on convection effects, further revealed the mechanisms influencing overall molecular uremic toxin removal performance. The results showed that design factors did not have a significant effect on LM removal performance; however, optimization of *PD* and *L*/*D* ratio could improve MM removal performance, enabling the same membrane to display greater effectiveness. In Chapter 4, the effects of *PD* and *L*/*D* ratio on hemodynamic stability and albumin filtration (albumin loss) performance were explored to characterize the relationships between design factors and the safety profile of CRRT filters. Through the construction of a comprehensive in vitro evaluation system that comprised continuous *TMP* monitoring, attenuation of hydraulic permeability, concentration polarization mass transfer resistance, albumin sieving coefficient over time, and amount of albumin removed, the mechanism of temporal protein filtration performance was analyzed; the impacts of design factors on the safety profile of CRRT filters were comprehensively evaluated. The results demonstrated that the optimization of design factors could effectively control the albumin filtration performance of CRRT filters; it could also improve the safety profile of CRRT filters. With the PSf hollow fiber membrane (d = 0.20 mm, Δx = 0.04 mm, k_{UF} = 22-23 mL/hr/mmHg, mean pore size = 5-6 nm), the LS-3 (*PD* = 60% and *L*/*D* ratio = 9.3) had the most optimal solute removal performance and safety profile. Chapter 5 explored the impacts of various design factors on internal filtration (convection effects), as well as the mechanisms that influence MM removal performance. Furthermore, experimental verification was conducted by constructing a multiple linear regression model of design factors and $Q_{\text{IF-Max}}$. Finally, an accurate and practical design equation was proposed to quantify the design factors influencing CRRT filters and convection effects: $Q_{\text{IF-Max}} = -34.775 + 4.749 \times \frac{N}{D^2} + 2.293 \times \frac{L}{D}$, where the impacts of N/D^2 and L/D ratio on $Q_{\text{IF-Max}}$ are 15.0%

and 85.0%, respectively. With the range of parameters evaluated in our study (CVVHD mode, Q_{BI} = 100 mL/min, Q_D = 16.7 mL/min (= 1000 mL/hr); PSf hollow fiber membrane (d = 0.20 mm, Δx = 0.04 mm, k_{UF} = 22-23 mL/hr/mmHg, mean pore size = 5-6 nm); *PD*, 50%-60%; *L*/*D* ratio, 2.9-9.3), the design equation is generalizable. Through simple substitution of design factor parameters without the requirement for filter sample production or experimental investigation, the proposed design equation was able to effectively quantify the convection effects of CRRT filters with different design factors, thereby predicting MM removal performance.

Considering the widespread application of CRRT in critical care medicine and nephrology, improvements in CRRT filter performance are expected to have major impacts on clinical treatment effectiveness. This study conducted a series of analyses concerning the impacts of design factors on CRRT filter performance and established a complete evaluation system, which has significant implications for the development of new CRRT filters.

Nomenclature

Q_B, blood flow rate [mL/min]

Q_{BI}, blood flow rate at the inlet of the filter [mL/min]

Q_{BO}, blood flow rate at the outlet of the filter [mL/min]

Q_D, dialysate flow rate [mL/min]

Q_F, filtrate flow rate [mL/min]

Q_{UF}, ultrafiltration flow rate [L/hr]

Q_R, replacement solution flow rate [L/hr]

d, inner diameter of hollow fiber [μm]

Δx, membrane thickness [μm]

L, effective length of hollow fiber [mm]

R_o, overall resistance of a solute to diffusion mass transfer by the filter [m^{-1}]

R_B, mass transfer resistance of the blood boundary layer [m^{-1}]

R_M, mass transfer resistance of the membrane itself [m^{-1}]

R_D, mass transfer resistance of the dialysate boundary layer [m^{-1}]

C_L, clearance [mL/min]

C_{BI}, sample concentration at the blood inlet [mmol/L]

C_{BO}, sample concentration at the blood outlet [mmol/L]

K_oA, overall mass transfer area coefficient [mL/min]

A, effective membrane area [m^2]

K_o, overall mass transfer coefficient [m/s]

K_B, mass transfer coefficient of the blood boundary layer [m/s]

K_M, mass transfer coefficient of the membrane itself [m/s]

K_D, mass transfer coefficient of the dialysate boundary layer [m/s]

A_o, nominal membrane surface area [m^2]

N, number of hollow fibers [-]

N_T, number of mass transfer units [-]

Z, blood flow to dialysate flow ratio [-]

E, dialysis efficiency [-]

$Q_{IF\text{-}Max}$, the maximum internal filtration flow rate [mL/min]

S, cross-sectional area of the hollow fibers [m^2]

Q_{BM}, the minimum blood flow rate [mL/min]

V_{BI}, inlet blood flow velocity [m/s]

V_{BM}, the minimum blood flow velocity [m/s]

ΔP_B, pressure drop on the blood side [Pa]

ΔP_D, pressure drop on the dialysate side [Pa]

P_{BI}, inlet pressure on the blood side [Pa]

P_{BO}, outlet pressure on the blood side [Pa]

P_{DI}, inlet pressure on the dialysate side [Pa]

P_{DO} outlet pressure on the dialysate side [Pa]

P_F, filtrate pressure [Pa]

μ_B, viscosities of the blood [Pa s]

μ_D, viscosities of the dialysate [Pa s]

D_e, equivalent diameter of the dialysate flow path [mm]

S_D, cross-sectional area of the dialysate flow path [m^2]

TMP, transmembrane pressure [mmHg]

k_{UF}, ultrafiltration coefficient [mL/(hr·mmHg)]

R_c, concentration polarization mass transfer resistance [m^{-1}]

R_t, total mass transfer resistance [m^{-1}]

R_f, mass transfer resistance of the protein cake layer [m^{-1}]

J, permeation flux [$L/m^2/hr$]

μ, filtrate viscosity of the membrane [Pa s]

SC, sieving coefficient [-]

C_F, protein concentration of the filtrate [mg/mL]

M_{fld}, amount of albumin filtered [mg]

D, inner diameter of the housing [mm]

PD, hollow fiber packing density [%]

b_1, regression coefficient of N/D^2 [mL·cm^2/min]

b_2, regression coefficient of L/D ratio [mL/min]

b_0, a constant term [mL/min]

β_1, standard coefficient of N/D^2 [-]

β_2, standard coefficient of L/D ratio [-]

References

1. Karkar A. Continuous renal replacement therapy: principles, modalities, and prescription. *Saudi J Kidney Dis Transpl* 2019; 30(6): 1201-1209.
2. Sribner BH, Caner JE, Buri R, Quinton W. The technique of continuous hemodialysis. *Trans Am Soc Artif Intern Organs* 1960; 6: 88-103.
3. Blagg CR. The early years of chronic dialysis: the Seattle contribution. *Am J Nephrol* 1999; 19(2): 350-354.
4. Henderson LW. Discovering the presence of convective transport: an artiphysiological moment in time. *Artif Organs* 2015; 39(12): 985-988.
5. Henderson LW, Besarab A, Michaels A, Bluemle LW Jr. Blood purification by ultrafiltration and fluid replacement (diafiltration). *Hemodial Int* 2004; 8(1): 10-18.
6. Kramer P, Wigger W, Rieger J, Matthaei D, Scheler F. Arteriovenous haemofiltration: a new and simple method for treatment of over-hydrated patients resistant to diuretics. *Klin Wochenschr* 1977; 55(22): 1121-1122.
7. Lauer A, Saccaggi A, Ronco C, Belledonne M, Glabman S, Bosch JP. Continuous arteriovenous hemofiltration in the critically ill patient. Clinical use and operational characteristics. *Ann Intern Med* 1983; 99(4): 455-460.
8. Ronco C, Bellomo R, Wratten ML, Tetta C. Future technology for continuous renal replacement therapies. *Am J of Kidney Dis* 1996; 28(5): 1269-1308.
9. Geronemus R and Schneider N. Continuous arteriovenous hemodialysis: a new modality for treatment of acute renal failure. *Trans Am Soc Artif Intern Organs* 1984; 30: 610-613.
10. Ronco C, Bragantini L, Brendolan A, Dell'Aquila R, Fabris A, Chiaramonte S, Feriani M, Laquaniti L, La Greca G. Arteriovenous hemodiafiltration (AVHDF) combined with continuous arteriovenous hemofiltration (CAVH). *Trans Am Soc Artif Intern Organs* 1985; 31: 349-353.
11. Ronco C and Bellomo R. Continuous renal replacement therapy: evolution in technology and current nomenclature. *Kidney Int Suppl* 1998; 66: 160-164.
12. Canaud B, Garred LJ, Christol JP, Aubas S, Béraud JJ, Mion C. Pump assisted continuous

venovenous hemofiltration for treating acute uremia. *Kidney Int Suppl* 1988; 24: 154-156.

13. Yorgin PD, Krensky AM, Tune BM. Continuous venovenous hemofiltration. *Pediatr Nephrol* 1990; 4: 640-642.
14. Macias WL, Mueller BA, Scarim SK, Robinson M, Rudy DW. Continuous venovenous hemofiltration: an alternative to continuous arteriovenous hemofiltration and hemodiafiltration in acute renal failure. *Am J Kidney Dis* 1991;18(4): 451-458.
15. Tam PY, Huraib S, Mahan B, LeBlanc D, Lunski CA, Holtzer C, Doyle CE, Vas SI, Uldall PR. Slow continuous hemodialysis for the management of complicated acute renal failure in an intensive care unit. *Clin Nephrol* 1988; 30(2): 79-85.
16. Ronco C. Continuous renal replacement therapies for the treatment of acute renal failure in intensive care patients. *Clin Nephrol* 1993; 40(4): 187-198.
17. Ronco C and Bellomo R. Critical care nephrology: the time has come. *Nephrol Dial Transplant* 1998; 13: 264-267.
18. Wendon J, Smithies M, Sheppard M, Bullen K, Tinker J, Bihari D. Continuous high volume venous-venous haemofiltration in acute renal failure. *Intensive Care Med* 1989; 15(6): 358-363.
19. Ronco C and Bellomo R. Continuous high flux dialysis: an efficient renal replacement, in Vincent JL (eds). Yearbook of Intensive Care and Emergency Medicine. Berlin, Germany, Springer, 1996; pp 690-696.
20. Tetta C, Cavaillon JM, Camussi G, Lonnemann FG, Brendolan A, Ronco C. Continuous plasma filtration coupled with sorbents. *Kidney Int Suppl* 1998; 66: S186-189.
21. Manns M, Sigler MH, Teehan BP. Continuous renal replacement therapies: an update. *Am J Kidney Dis* 1998; 32(2): 185-207.
22. Ricci Z, Bonello M, Salvatori G, Ratanarat R, Brendolan A, Dan M, Bellomo R, Ronco C. Continuous renal replacement technology: from adaptive technology and early dedicated machines towards flexible multipurpose machine platforms. *Blood Purif* 2004; 22(3): 269-276.
23. Ronco C. Continuous renal replacement therapy: forty-year anniversary. *Int J Artif Organs* 2017; 40(6): 257-264.

24. Bellomo R, Ronco C, Mehta RL. Nomenclature for continuous renal replacement therapies. *Am J Kidney Dis* 1996; 28(5): 2-7.
25. Ronco C and Bellomo R. Basic mechanisms and definitions for continuous renal replacement therapies. *Int J Artif Organs* 1996; 19(2): 95-99.
26. Ronco C and Bellomo R. Acute renal failure and multiple organ dysfunction in the ICU: from renal replacement therapy (RRT) to multiple organ support therapy (MOST). *Int J Artif Organs* 2002; 25(8): 733-747.
27. Mehta RL. Continuous renal replacement therapy in the critically ill patient. *Kidney Int* 2005; 67(2): 781-795.
28. Grootendorst AF and van Bommel EF. The role of hemofiltration in the critically-ill intensive care unit patient: present and future. *Blood Purif* 1993; 11(4): 209-223.
29. Hirasawa H, Sugai T, Ohtake Y, Oda S, Matsuda K, Kitamura N. Blood purification for prevention and treatment of multiple organ failure. *World J Surg* 1996; 20(4): 482-486.
30. Ronco C and Bellomo R. New CRRT systems: impact on dose delivery. *Am J Kidney Dis* 1997; 30(5 Suppl 4): 15-19.
31. Rimmelé T and Kellum JA. High-volume hemofiltration in the intensive care unit: a blood purification therapy. *Anesthesiology* 2012; 116(6): 1377-1387.
32. Ronco C, Bellomo R, Hensel M. Continuous "high flux" dialysis: an effective renal replacement therapy for intensive care patients. *Zentralbl Chir* 1997; 122(5): 378-382.
33. Ronco C. Recent evolution of renal replacement therapy in the critically ill patient. *Crit Care* 2006; 10(1): 123.
34. Clark WR, Gao D, Lorenzin A, Ronco C. Membranes and Sorbents. *Contrib Nephrol* 2018; 194: 70-79.
35. Yamashita AC and Kawanishi H. Kinetic analysis of daily hemofiltration. *Hemodial Int* 2004; 8: 326-331.
36. Bellomo R and Ronco C. Acute renal failure in the intensive care unit: adequacy of dialysis and the case for continuous therapies. *Nephrol Dial Transplant* 1996; 11(3): 424-428.
37. Ji DX, Gong DH, Xu B, Tao J, Ren B, Zhang YD, Liu Y, Hu WX, Wang MM, Li LS. Continuous veno-venous hemofiltration in the treatment of acute severe hyponatremia: a

report of 11 cases. *Int J Artif Organs* 2007; 30(2): 176-180.

38. Abuelo JG, Shemin D, Chazan JA. Acute symptoms produced by hemodialysis: a review of their causes and associations. *Semin Dial* 1993; 6: 59-69.
39. Daugirdas JT. Pathophysiology of dialysis hypotension: an update. *Am J Kidney Dis* 2001; 38(4 Suppl 4): S11-17.
40. Sigwalt F, Bouteleux A, Dambricourt F, Asselborn T, Moriceau F, Rimmelé T. Clinical complications of continuous renal replacement therapy. *Contrib Nephrol* 2018; 194: 109-117.
41. Kim SG, Yun D, Lee J, Kim YC, Kim DK, Oh KH, Joo KW, Kim YS, Han SS. Impact of intradialytic hypotension on mortality following the transition from continuous renal replacement therapy to intermittent hemodialysis. *Acute Crit Care* 2022; 38(1): 86-94.
42. Manns M, Sigler MH, Teehan BP. Intradialytic renal haemodynamics-potential consequences for the management of the patient with acute renal failure. *Nephrol Dial Transplant* 1997; 12(5): 870-872.
43. Manns M, Sigler MH, Teehan BP. Advantages of continuous veno-venous hemodialysis (CVVHD) in acute renal failure. *J Am Soc Nephrol* 1995; 16: 470.
44. Tandukar S and Palevsky PM. Continuous renal replacement therapy: who, when, why, and how. *Chest* 2019; 155(3): 626-638.
45. Chen J-j, Li H and Chen L-l. The research progress of fluid balance management of continuous renal replacement therapy. *Chinese Nursing Management* 2013; 13(1); 104-107.
46. Bouchard J and Mehta RL. Volume management in continuous renal replacement therapy. *Semin Dial* 2009; 22(2): 146-150.
47. Bellomo R, Mansfield D, Rumble S, Shapiro J, Parkin G, Boyce N. Acute renal failure in critical illness. Conventional dialysis versus acute continuous hemodiafiltration. *ASAIO J* 1992; 38(3): M654-657.
48. McDonald BR and Mehta RL. Decreased mortality in patients with acute renal failure undergoing continuous arteriovenous hemodialysis. *Contrib Nephrol* 1991; 93: 51-56.
49. Monson P and Mehta RL. Nutrition in acute renal failure: a reappraisal for the 1990s. *J Renal Nutr* 1994; 4: 58-77.
50. Cerdá J and Ronco C. Modalities of continuous renal replacement therapy: technical and

clinical considerations. *Semin Dial* 2009; 22(2): 114-122.

51. Kellum JA, Romagnani P, Ashuntantang G, Ronco C, Zarbock A, Anders HJ. Acute kidney injury. *Nat Rev Dis Primers* 2021; 7(1): 52.
52. Cerdá J, Bagga A, Kher V, Chakravarthi RM. The contrasting characteristics of acute kidney injury in developed and developing countries. *Nat Clin Pract Nephrol* 2008; 4(3): 138-153.
53. Schoenfelder T, Chen X, Bleß HH. Effects of continuous and intermittent renal replacement therapies among adult patients with acute kidney injury. *GMS Health Technol Assess* 2017; 13: Doc01.
54. de Mendonça A, Vincent JL, Suter PM, Moreno R, Dearden NM, Antonelli M, Takala J, Sprung C, Cantraine F. Acute renal failure in the ICU: risk factors and outcome evaluated by the SOFA score. *Intensive Care Med* 2000; 26(7): 915-921.
55. Susantitaphong P, Cruz DN, Cerda J, Abulfaraj M, Alqahtani F, Koulouridis I, Jaber BL; Acute Kidney Injury Advisory Group of the American Society of Nephrology. World incidence of AKI: a meta-analysis. *Clin J Am Soc Nephrol* 2013; 8(9): 1482-1493.
56. Ricci Z, Romagnoli S, Ronco C. Acute kidney injury: to dialyse or to filter? *Nephrol Dial Transplant* 2020; 35(1): 44-46.
57. Davenport A. Renal replacement therapy for the patient with acute traumatic brain injury and severe acute kidney injury. *Contrib Nephrol* 2007; 156: 333-339.
58. Walsh CR. Multiple organ dysfunction syndrome after multiple trauma. *Orthop Nurs* 2005; 24(5): 324-333.
59. Angus DC, Linde-Zwirble WT, Lidicker J, Clermont G, Carcillo J, Pinsky MR. Epidemiology of severe sepsis in the United States: analysis of incidence, outcome, and associated costs of care. *Crit Care Med* 2001; 29(7): 1303-1310.
60. Joannidis M. Continuous renal replacement therapy in sepsis and multisystem organ failure. *Semin Dial* 2009; 22(2): 160-164.
61. Oda S, Sadahiro T, Hirayama Y, Nakamura M, Watanabe E, Tateishi Y, Hirasawa H. Non-renal indications for continuous renal replacement therapy: current status in Japan. *Contrib Nephrol* 2010; 166: 47-53.
62. Peng Z, Pai P, Hong-Bao L, Rong L, Han-Min W, Chen H. The impacts of continuous veno-

venous hemofiltration on plasma cytokines and monocyte human leukocyte antigen-DR expression in septic patients. *Cytokine* 2010; 50(2): 186-191.

63. Cole L, Bellomo R, Journois D, Davenport P, Baldwin I, Tipping P. High-volume haemofiltration in human septic shock. *Intensive Care Med* 2001; 27(6): 978-986.
64. Ha SO, Kim HS, Park S, Jung KS, Jang SH, Han SJ, Kim HS, Lee SH. Severe ARDS caused by adenovirus: early initiation of ECMO plus continuous renal replacement therapy. *Springerplus* 2016; 5(1): 1909.
65. Yu C, Liu Z, Gong D, Ji D, Li L. The monocyte dysfunction induced by acute tetramine poisoning and corrected by continuous blood purification. *Arch Toxicol* 2005; 79(1): 47-53.
66. Dehua G, Daxi J, Honglang X, Bin X, Yun L, Leishi L. Sequential hemoperfusion and continuous venovenous hemofiltration in treatment of severe tetramine poisoning. *Blood Purif* 2006; 24(5-6): 524-530.
67. Kolff WJ, Berk HT, ter Welle M, van der LEY AJ, van Dijk EC, van Noordwijk J. The artificial kidney: a dialyser with a great area. *J Am Soc Nephrol* 1997; 8(12): 1959-1965.
68. Kolff WJ, Watschinger B, Vertes V. Results in patients treated with the coil kidney (disposable dialyzing unit). *J Am Med Assoc* 1956; 161(15): 1433-1437.
69. Kiil F. Development of a parallel-flow artificial kidney in plastics. *Acta Chir Scand Suppl* 1960; Suppl 253: 142-150.
70. Gotch F, Lipps B, Weaver J Jr, Brandes J, Rosin J, Sargent J, Oja P. Chronic hemodialysis with the hollow fiber artificial kidney (HFAK). *Trans Am Soc Artif Intern Organs* 1969; 15: 87-96.
71. Sakai K. Dialysis membranes for blood purification. *Frontiers Med Biol Eng* 2000; 10(2): 117-129.
72. Clark WR, Gao D, Lorenzin A, Ronco C. Membranes and Sorbents. *Contrib Nephrol* 2018; 194: 70-79.
73. Vanholder R, Glorieux G, De Smet R, Lameire N; European Uremic Toxin Work Group. New insights in uremic toxins. *Kidney Int Suppl* 2003; 84: 6-10.
74. Rosner MH, Reis T, Husain-Syed F, Vanholder R, Hutchison C, Stenvinkel P, Blankestijn PJ, Cozzolino M, Juillard L, Kashani K, Kaushik M, Kawanishi H, Massy Z, Sirich TL, Zuo L,

Ronco C. Classification of uremic toxins and their role in kidney failure. *Clin J Am Soc Nephrol* 2021; 16(12): 1918-1928.

75. Claure-Del Granado R, Clark WR. Continuous renal replacement therapy principles. *Semin Dial* 2021; 34(6): 398-405.
76. Huang Z, Clark WR, Gao D. Determinants of small solute clearance in hemodialysis. *Semin Dial* 2005; 18(1): 30-35.
77. Colton CK, Henderson LW, Ford CA, Lysaght MJ. Kinetics of hemodiafiltration. I. In vitro transport characteristics of a hollow-fiber blood ultrafilter. *J Lab Clin Med* 1975; 85(3): 355-371.
78. O'Reilly P and Tolwani A. Renal replacement therapy III: IHD, CRRT, SLED. *Crit Care Clin* 2005; 21(2): 367-378.
79. Vigan ò SM, Di Filippo S, Manzoni C, Locatelli F. Membrane characteristics. *Contrib Nephrol* 2008; 161: 162-167.
80. ISO, 8637-1:2017, Extracorporeal systems for blood purification-Part 1: haemodialysers, haemodiafilters, haemofilters and haemoconcentrators.
81. Leypoldt JK and Cheung AK. Optimal use of hemodialyzers. *Contrib Nephrol* 2002; 137: 129-137.
82. Ward RA, Leypoldt JK, Clark WR, Ronco C, Mishkin GJ, Paganini EP. What clinically important advances in understanding and improving dialyzer function have occurred recently? *Semin Dial* 2001; 14(3): 160-174.
83. Fukuda M, Yoshimura K, Namekawa K, Sakai K. Technical characterization of dialysis fluid flow and mass transfer rate in dialyzers with various filtration coefficients using dimensionless correlation equation. *J Artif Organs* 2017; 20(2): 145-151.
84. Mineshima M. Optimal design of dialyzers. *Contrib Nephrol* 2017; 189: 204-209.
85. Sato Y, Mineshima M, Ishimori I, Kaneko I, Akiba T, Teraoka S. Effect of hollow fiber length on solute removal and quantification of internal filtration rate by Doppler ultrasound. *Int J Artif Organs* 2003; 26(2): 129-134.
86. Sakiyama R, Ishimori I, Akiba T, Mineshima M. Effect of blood flow rate on internal filtration in a high-flux dialyzer with polysulfone membrane. *J Artif Organs* 2012; 15(3):

266-271.

87. Mineshima M, Ishimori I, Ishida K, Hoshino T, Kaneko I, Sato Y, Agishi T, Tamamura N, Sakurai H, Masuda T, Hattori H. Effects of internal filtration on the solute removal efficiency of a dialyzer. *ASAIO J* 2000; 46(4): 456-460.
88. Luis P. Fundamental Modelling of Membrane Systems. 2018, p.13-18.
89. Ronco C. Hemodiafiltration: technical and clinical issues. *Blood Purif* 2015; 40(Suppl 1): 2-11.
90. Ho C-C and Zydney AL. Transmembrane pressure profiles during constant flux microfiltration of bovine serum albumin. *J Membr Sci* 2002; 209: 363-377.
91. Kosaku T, Tomisawa N, Iwashima S, Jimbo Y, Yamashita AC. The influence of design factors of diafilters on the amount of albumin leakage. *JSBPCC* 2017; 8(1): 54-57.
92. Miller DJ, Kasemset S, Paul DR. Freeman BD. Comparison of membrane fouling at constant flux and constant transmembrane pressure conditions. J Membr Sci 2014; 454: 505-515.
93. Choi H, Zhang K, Dionysiou DD, Oerther DB, Sorial GA. Influence of cross-flow velocity on membrane performance during filtration of biological suspension. J Membr Sci 2015; 248: 189-199.
94. Hulko M, Haug U, Gauss J, Boschetti-de-Fierro A, Beck W, Krause B. Requirements and pitfalls of dialyzer sieving coefficients comparisons. *Artif Organs* 2018; 42(12): 1164-1173.
95. Ronco C and Clark WR. Haemodialysis membranes. *Nat Rev Nephrol*. 2018; 14(6): 394-410.
96. Dammacco F, Miglietta A, Bonomo L. Analbuminemia (a quantitative albumin variant). *Ric Clin Lab* 1979; 9(1): 5-12.
97. Douvris A, Malhi G, Hiremath S, McIntyre L, Silver SA, Bagshaw SM, Wald R, Ronco C, Sikora L, Weber C, Clark EG. Interventions to prevent hemodynamic instability during renal replacement therapy in critically ill patients: a systematic review. *Crit Care* 2018; 22(1): 41.
98. Hakim RM, Fearon DT, Lazarus JM. Biocompatibility of dialysis membranes: effects of chronic complement activation. *Kidney Int* 1984; 26(2): 194-200.
99. Hakim RM. Clinical implications of hemodialysis membrane biocompatibility. *Kidney Int* 1993; 44(3): 484-494.
100. Sunohara T and Masuda T. Cellulose triacetate as a high-performance membrane. *Contrib*

Nephrol 2011; 173: 156-163.

101. Pichaiwong W, Leelahavanichkul A, Eiam-Ong S. Efficacy of cellulose triacetate dialyzer and polysulfone synthetic hemofilter for continuous veno-venous hemofiltration in acute renal failure. *J Med Assoc Thai* 2006, 89 Suppl 2: S65-72.
102. Kohlová M, Amorim CG, Araújo A, Santos-Silva A, Solich P, Montenegro MCBSM. The biocompatibility and bioactivity of hemodialysis membranes: their impact in end-stage renal disease. *J Artif Organs* 2019; 22(1): 14-28.
103. Gejyo F, Yamada T, Odani S, Nakagawa Y, Arakawa M, Kunitomo T, Kataoka H, Suzuki M, Hirasawa Y, Shirahama T. A new form of amyloid protein associated with chronic hemodialysis was identified as beta 2-microglobulin. *Biochem Biophys Res Commun* 1985; 129(3): 701-706.
104. Abe M, Masakane I, Wada A, Nakai S, Nitta K, Nakamoto H. Dialyzer classification and mortality in hemodialysis patients: a 3-year nationwide cohort study. *Front Med (Lausanne)* 2021; 8: 740461.
105. Cuker A and Cines DB. How I treat heparin-induced thrombocytopenia. *Blood* 2012; 119(10): 2209-2218.
106. Ren X, Xu L, Xu J, Zhu P, Zuo L, Wei S. Immobilized heparin and its anti-coagulation effect on polysulfone membrane surface. *J Biomater Sci Polym Ed* 2013; 24(15): 1707-1720.
107. Hirayama T, Nosaka N, Okawa Y, Ushio S, Kitamura Y, Sendo T, Ugawa T, Nakao A. AN69ST membranes adsorb nafamostat mesylate and affect the management of anticoagulant therapy: a retrospective study. *J Intensive Care* 2017; 5: 46.
108. Stasi A, Franzin R, Divella C, Sallustio F, Curci C, Picerno A, Pontrelli P, Staffieri F, Lacitignola L, Crovace A, Cantaluppi V, Medica D, Ronco C, de Cal M, Lorenzin A, Zanella M, Pertosa GB, Stallone G, Gesualdo L, Castellano G. PMMA-based continuous hemofiltration modulated complement activation and renal dysfunction in LPS-induced acute kidney injury. *Front Immunol* 2021; 12: 605212.
109. Ronco C, Brendolan A, Crepaldi C, Rodighiero M, Scabardi M. Blood and dialysate flow distributions in hollow-fiber hemodialyzers analyzed by computerized helical scanning technique. *J Am Soc Nephrol* 2002; 13(Suppl 1): 53-61.

110. Fukuda M, Miyazaki M, Uezumi S, Yoshida M. Design and assessment of the new APS dialyzer (APS-SA series). *J Artif Organs* 2006; 9(3): 192-198.
111. Yamamoto K, Matsuda M, Hirano A, Takizawa N, Iwashima S, Yakushiji T, Fukuda M, Miyasaka T, Sakai K. Computational evaluation of dialysis fluid flow in dialyzers with variously designed jackets. *Artif Organs* 2009; 33(6): 481-486.
112. Hirano A, Yamamoto K, Matsuda M, Ogawa T, Yakushiji T, Miyasaka T, Sakai K. Evaluation of dialyzer jacket structure and hollow-fiber dialysis membranes to achieve high dialysis performance. *Ther Apher Dial* 2011; 15(1): 66-74.
113. Nguyen T-T, Jang K, Her N, Kim CS, Kim SW, Kim InS. Fabrication of hollow fiber membranes with different inner diameters for enhanced uremic toxins removal in hemodialysis: exploring from high-flux to high molecular weight retention onset classes. *J Membr Sci* 2022; 663: 121065.
114. Ronco C, Brendolan A, Lupi A, Metry G, Levin NW. Effects of a reduced inner diameter of hollow fibers in hemodialyzers. *Kidney Int* 2000; 58(2): 809-817.
115. Raff M, Welsch M, Göhl H, Hildwein H, Storr M, Wittner B. Advanced modeling of highflux hemodialysis. *J Membr Sci* 2003; 216: 1-11.
116. Sato Y, Mineshima M, Ishimori I, Kaneko I, Akiba T, Teraoka S. Effect of hollow fiber length on solute removal and quantification of internal filtration rate by Doppler ultrasound. *Int J Artif Organs* 2003; 26(2): 129-134.
117. Ronco C, Ballestri M, Brendolan A. New developments in hemodialyzers. *Blood Purif* 2000; 18(4): 267-275.
118. Hirano A, Kida S, Yamamoto K, Sakai K. Experimental evaluation of flow and dialysis performance of hollow-fiber dialyzers with different packing densities. *J Artif Organs* 2012; 15(2): 168-175.
119. Donato D, Storr M, Krause B. Design optimization of hollow fiber dialyzers to enhance internal filtration based on a mathematical model. *J Membr Sci* 2020; 598: 117690.
120. Suzuki Y, Kohori F, Sakai K. Computer-aided design of hollow-fiber dialyzers. *J Artif Organs* 2001; 4: 326-333.
121. Donato D, Boschetti-de-Fierro A, Zweigart C, Kolb M, Eloot S, Storr M, Krause B, Leypoldt

K, Segers P. Optimization of dialyzer design to maximize solute removal with a two-dimensional transport model. *J Membr Sci* 2017; 541: 519-528.

122. Yamashita AC, Fujita R, Tomisawa N, Jinbo Y, Yamamura M. Effect of packing density of hollow fibers on solute removal performances of dialyzers. *Hemodial Int* 2009; 13 Suppl 1: S2-7.
123. Clark WR, Leblanc M, Levin NW. The acute dialysis quality initiative-Part IV: Membranes for CRRT. *Adv Ren Replace Ther* 2002; 9(4): 265-267.
124. Weidhase L, de Fallois J, Hauß ig E, Kaiser T, Mende M, Petros S. Myoglobin clearance with continuous veno-venous hemodialysis using high cutoff dialyzer versus continuous veno-venous hemodiafiltration using high-flux dialyzer: a prospective randomized controlled trial. *Crit Care* 2020; 24(1): 644.
125. Douvris A, Zeid K, Hiremath S. Bagshaw SM, Wald R, Beaubien-Souligny W, Kong J, Ronco C, Clark EG. Mechanisms for hemodynamic instability related to renal replacement therapy: a narrative review. *Intensive Care Med* 2019; 45(10): 1333-1346.
126. Portales-Castillo I, Yee J, Tanaka H, Fenves AZ. Beta-2 Microglobulin Amyloidosis: Past, Present, and Future. *Kidney 360* 2020; 1(12): 1447-1455.
127. Jadoul M and Drüeke TB. β_2 microglobulin amyloidosis: an update 30 years later. *Nephrol Dial Transplant* 2016; 31(4): 507-509.
128. Liabeuf S, Lenglet A, Desjardins L, Neirynck N, Glorieux G, Lemke HD, Vanholder R, Diouf M, Choukroun G, Massy ZA; European Uremic Toxin Work Group (EUTox). Plasma beta-2 microglobulin is associated with cardiovascular disease in uremic patients. *Kidney Int* 2012; 82(12):1297-1303.
129. Petejova N and Martinek A. Acute kidney injury due to rhabdomyolysis and renal replacement therapy: a critical review. *Crit Care* 2014; 18(3): 224.
130. Premru V, Kovač J, Ponikvar R. Use of myoglobin as a marker and predictor in myoglobinuric acute kidney injury. *Ther Apher Dial* 2013; 17(4): 391-395.
131. Xie F and Ye X. Study on optimum separate technique of Agarcus blazei Murill (ADM) polysaccharides with PS ultrafiltration membrane by uniform design method. *JFST* 2010; 35(5): 120-123.

132. Wang Y, Wang S, Zhang J, Zhang M, Zhang H, Gong G, Luo M, Wang T, Mao X. Salusin-β is superior to salusin-α as a marker for evaluating coronary atherosclerosis. *J Int Med Res* 2020; 48(2): 300060520903868.
133. Sadiq IA and Komali K. On the study of clear causal risk factors of diabetes mellitus using multiple regression. *AJPAS* 2020; 9(4): 29-47.
134. Riley RD, Snell KI, Ensor J, Burke DL, Harrell FE Jr, Moons KG, Collins GS. Minimum sample size for developing a multivariable prediction model: PART II-binary and time-to-event outcomes. *Stat Med* 2019; 38(7): 1276-1296.

Acknowledgments

First and foremost, I would like to express my sincere gratitude to Professor Yamashita Akihiro C., who provided me with precise guidance from the inception of the research plan to the final paper revision. His profound expertise and unwavering dedication as a distinguished expert and top-notch scholar in the field have set a remarkable example for my future research endeavors. I aspire to follow in Professor Yamashita's footsteps and champion the application of chemical engineering in dialysis therapy, continuously developing innovative solutions aligned with clinical needs to enhance patient quality of life and treatment effectiveness.

I extend my heartfelt appreciation to Ms. Zhang Lin and Ms. Yu Yanan for their invaluable collaboration this journey, during which we overcame numerous challenges. Your relentless efforts have deeply touched me.

I must also acknowledge the invaluable support and encouragement of Professor Ijima Hiroyuki from the Engineering Department of Kyushu University and Assistant Professor Fumi Irie from the Medical Sciences Department. Their guidance was instrumental in my work.

Lastly, my profound thanks go to my parents, especially my mother, whose unwavering maternal love has been my constant support. I hope that my love and dedication can also illuminate my child's path to success.

May our hearts be filled with love, and may our endeavors bring light to the world, making it a better place through our collective efforts.

Changjun Mu

Monday, September 25, 2023